Desalination 583 (2024) 117724

Contents lists available at ScienceDirect

Desalination

journal homepage: www.elsevier.com/locate/desal

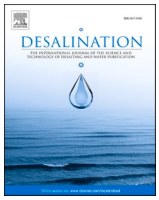

# Multi-scale modelling of an electrodialysis with bipolar membranes pilot plant and economic evaluation of its potential

Giovanni Virruso [a], Calogero Cassaro [a], Andrea Culcasi [a], Andrea Cipollina [a,*], Alessandro Tamburini [a], I. David L. Bogle [b], Giorgio D.M. Micale [a]

[a] Dipartimento di ingegneria, Università degli studi di Palermo, Viale delle scienze Ed.6, Palermo 90128, Italy
[b] Centre for Process Systems Engineering, Department of Chemical Engineering, University College London, Torrington Place, London WC1E 7JE, United Kingdom

ARTICLE INFO

*Keywords:*
BMED
Ion-exchange membrane
Model
Parasitic currents
Techno-economic analysis
Scale-up

ABSTRACT

Sodium hydroxide and hydrochloric acid are widely used chemicals in different industrial sectors. To minimize costs and risks associated with transportation, handling and storage, these hazardous chemicals can be produced in situ employing electrodialysis with bipolar membranes (EDBM). This work presents a multi-scale model capable of simulating large scale EDBM units with complex stack configuration (i.e., internal staging) that can be used to design and optimize the process. The model was validated in two different process configurations using experimental results obtained from an EDBM pilot plant. Discrepancies between model and experimental results in the range of 2–11 % were obtained. The validated model was used to conduct a techno-economic evaluation adopting the feed and bleed configuration. Results show that current efficiency increases as the current density rises. At 600 A $m^{-2}$, values of current efficiency between 72 % and 96 % were found for sodium hydroxide concentration in the range of 0.5–1 mol $L^{-1}$. The levelized cost of sodium hydroxide (LCoNaOH) was evaluated, in the same range of concentrations, demonstrating that values between 280 and 370 € $ton^{-1}$ can be obtained, fixing the electricity prince (0.1 kWh $kg^{-1}$) and the triplet specific cost (600 US$ $m^{-2}$). Moreover, assuming a reduced cost of electricity and triplet to 0.05 kWh $kg^{-1}$ and 300 US$ $m^{-2}$, respectively, an absolute minimum of 140 € $ton^{-1}$ was found for the target 0.5 mol $L^{-1}$. A double stage EDBM configuration was simulated to show the scale-up potentials of the multi-scale model. A reduction in the LcoNaOH of 10 % was obtained for a target concentration of 1 mol $L^{-1}$. These results prove the attractiveness of the EDBM technology for producing in situ chemicals.

## 1. Introduction

Sodium hydroxide and hydrochloric acid represent two of the most widely used bulk industrial chemicals available on the market. They are employed across different industrial sectors and, in almost all applications, they are utilized as solutions with concentrations ranging from 1 to 30 wt%. Sodium hydroxide, also known as caustic soda, is mainly employed for neutralization purposes or as a reaction medium [1]. Approximately 99.5 % of caustic soda worldwide is produced utilizing the traditional chlor-alkali process [2]. In 2021, approximately 9.000 kton of sodium hydroxide were employed in Europe [3]. Sodium hydroxide in mainly used in the pulp and paper industry, in the organic and inorganic chemical industries, as well as in the textile and aluminium sectors, overall accounting for 65 % of the total production [4]. For these applications, concentrated solutions between 10 and 30 wt% are employed. Moreover, a number of important applications use low concentrated NaOH solutions. Water treatment and food industries represented 5.1 % and 6.4 % respectively of the applications of caustic soda in Europe [3]. In the water treatment industry sodium hydroxide is primarily utilized for pH adjustment [5], membrane cleaning [6] and the regeneration of ion-exchange resins [7]. For these applications lower solution concentrations of 1–4 wt% are preferred. In the field of brine valorisation sodium hydroxide is employed in the production of Mg $(OH)_2$ and $Ca(OH)_2$ from waste salt solutions using innovative crystallizers [8]. In the food industries caustic soda is used for cleaning procedures and for the production of starches and derivatives [9]. Notably, vinegar residue, a by-product of vinegar manufacturing, can be pretreated with a 3 wt% NaOH solution before anaerobic digestion to

* Corresponding author.
*E-mail address:* andrea.cipollina@unipa.it (A. Cipollina).

https://doi.org/10.1016/j.desal.2024.117724
Received 4 January 2024; Received in revised form 5 April 2024; Accepted 3 May 2024
Available online 6 May 2024

enhance methane production by 54 % [10]. Sodium hydroxide is also considered an attractive absorbent for $CO_2$ as it converts the latter into sodium carbonate which has high stability, minimal environmental impact, and low cost [11]. For this purpose, 1–8 wt% sodium hydroxide solutions are commonly used [12,13].

Aqueous solutions of hydrochloric acid also have many industrial applications. These solutions are primarily obtained from the organic chlorination sector, especially from vinyl chloride production [4]. The main applications include chloride manufacture, mineral dissolution, pickling and etching of metals, alkaline stream neutralization, brine acidification, regeneration process, cleaning procedures as well as production of plastics, cosmetic and detergent [4,14,15]. The hydrochloric acid pickling process is widely adopted in the steel manufacturing industry to remove oxidized layers from steel surfaces. Depending on the process conditions, HCl solution concentrations between 1.5 and 17 wt % are employed [16]. Hydrochloric acid is also used as a solvent in leaching processes focusing on aluminium recovery from sludge produced by water treatment plants. For these purposes HCl concentrations between 1 and 4 mol $L^{-1}$ are usually adopted leading to leaching efficiencies between 72 and 80 % [17]. In the food industry low-concentrated hydrochloric acid solutions are utilized to produce corn syrups, gelatin, hydrolysed vegetable protein, and soy sauces [14]. As a food additive HCl is known as E 507. In the field of ion exchange resin regeneration, especially for strong acid cation exchange resins, hydrochloric acid solutions are employed with a concentration of approximatively 4 wt% [18].

Often, when a strong base is used, it is also necessary to work with an acid solution, and vice-versa, to allow for pH control, neutralization of effluents, and cleaning processes.

These chemicals are produced as commodities in large volumes in specific industrial regions and they must be concentrated to reduce transport volume for ease of selling and shipping worldwide. However, due to the hazard they pose to human health they must be handled with care, and some concerns arise from environmental and social perspectives. Moreover, concentration and transportation account for a significant fraction of the total cost. In remote areas, such as islands, inland areas and the countryside, these issues are exacerbated. As an example, these chemicals are needed in all desalination plants to perform membrane cleaning and pH adjustments. Often these desalination plants are located on small islands and obtaining these chemicals can thus be quite expensive and, in addition, safe storage is needed. All these aspects highlight the necessity for a safe, sustainable and cost-effective method for the in situ production of hydrochloric acid and sodium hydroxide.

Electrodialysis with bipolar membranes (EDBM) represents one of the most promising technologies to tackle these issues. Indeed, by means of this technology both chemicals are simultaneously produced starting from the corresponding salt (i.e., sodium chloride) solution [19]. EDBM adopts three different types of ion-exchange membranes: the cation exchange membrane (CEM), anion exchange membrane (AEM) and bipolar membrane (BPM). The BPM, a laminate of cation (CEL) and anion exchange layers (AEL), is the key element of the process [20]. The region formed between the two ion-exchange layers is called the interlayer or transition region. The membranes are stacked together with polymeric spacers, placed between them, to generate solution channels, ensuring that the AEL of the bipolar membrane faces the CEM. The channel formed between the monopolar membranes (i.e., CEM and AEM) is the salt channel, while the two channels between the CEL and AEM as well as between the AEL and CEM represent the acid and base channels, respectively [21]. The three formed channels and the three different membranes represent the repetitive unit of the EDBM technology, which is called triplet. When stacking triplets together and supplying a direct current through the system, using a pair of electrodes placed at either end, chemical production and salt solution desalination can be performed concurrently. The main phenomena responsible for these processes are ion migration and water dissociation reaction, occurring in the transition region of the bipolar membrane. Cations migrate towards the cathode (negatively charged electrode) while anions migrate towards the anode (positively charged electrode). Ion migration is allowed or hindered depending on the polarity of the fixed charges contained in the membranes, e.g. cations can easily pass through CEM but they are retained by AEM, and vice versa for the anions [19]. Water dissociation reaction, which produces protons and hydroxide ions, is often promoted employing weak acid or base catalysts [22]. In such a way, protons and anions coming from the salt stream form an acid solution in the acid compartment, while, in a similar way, hydroxide ions and cations coming from the salt solution produce an alkaline solution in the base compartment. Typical operative range for EDBM units spam between 100 and 1000 A $m^{-2}$, while the voltage drops depends on the number of repetitive units installed in the stack, with values up to a few volts per triplet [19]. A schematic representation of an EDBM unit is presented in Fig. 1a.

The EDBM technology has been widely investigated by experimental works in different fields [23,24], but only a few focused on pilot plant units with large membrane areas [25–27]. Regarding the modelling of these systems, several works have been published, and a comprehensive review has been presented by Culcasi et al. [28]. Apart from a few works that computed local mass balances [28–30], all the other models reported so far adopted a simplified approach with lumped parameters [31] or the computation of global mass balances [32,33]. The Nernst-Planck approach is widely used to estimate trans-membrane fluxes [28,30,31], while the non-equilibrium thermodynamics (NET) approach is seldom adopted [29]. Concentration polarization causes a difference in concentration between the bulk of the solution and the solution-side of the solution-membrane interface. This effect is caused by the higher transport number of counter-ions in the membrane phase than in the solution phase [19]. To predict this effect, a few studies have applied Donnan equilibria [28,29,34]. Additionally, the concentration polarization effect may have significant implications, especially for the salt compartment, where these phenomena can support the achievement of the diffusion-limited current due to the concentration at the solution side of the solution-membrane interface becoming zero [19]. In addition, osmotic and electro-osmotic water fluxes have rarely been considered, even though they can lead to significant variations in the volumes and concentrations of the solutions [28,33]. Parasitic currents, also referred to as leakage currents, are detrimental phenomena that reduce the current utilization of the system and are generated by the presence of alternative paths for the ion current. These paths arise from the parallel hydraulic connection between the triplets. Consequently, solution channels of the same type are also connected through collectors and distributors (also known as manifolds) which act as salt-bridges and prevent a portion of the useful ion current from passing through the active membrane area. As a result, the ionic current flowing through the manifolds diminishes the effective current across the membranes responsible for chemicals production and desalination. Therefore, assessing parasitic currents is crucial, especially in industrial applications where energetic consumption is an important consideration. Only one previous study included parasitic currents in an EDBM model [28]. It was found that the effect of parasitic currents is exacerbated as the resistance of the cell pack increases [35] and, thus, for industrial scale EDBM stacks their effect must be considered.

Some of the models reported so far in the literature have been validated with experimental results. In Table 1, a list of these models is reported showing the operating conditions and the process configurations adopted to validate them. In some cases, a wide range of current densities was utilized [31,32], while others adopted only one current density value [28,33]. In almost all previous studies the range of acid and base concentrations used for validation was between 0.1 and 1 mol $L^{-1}$, with only a few exceptions [28,30]. Moreover, all the studies adopted only closed-loop process configurations in lab-scale EDBM units. Indeed, the number of triplets installed ranges between 1 and 5 with an active membrane area in the range of 0.004–0.028 $m^2$. The EDBM process has been demonstrated to be more effective for low outlet

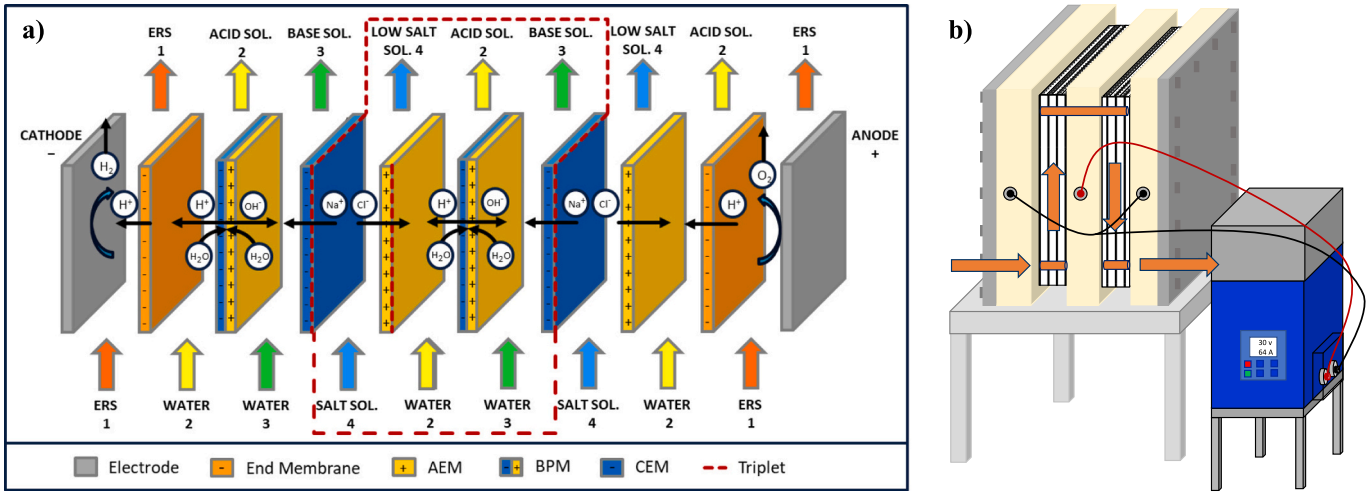


**Fig. 1.** a) Key elements and working principle of an EDBM stack. All the four solutions circulating in the stack are shown. ERS: electrode rinse solution. b) Schematic representation of an EDBM stack adopting an internal staging configuration with a shared anode. The arrows represent the inlet/outlet of the three main solutions (i.e., acid, base and salt).

**Table 1**
List of the models reported in literature, showing the processes configurations and operating conditions adopted to validation them in comparison with the present work.

| Reference | Validation range | | | | | | |
|---|---|---|---|---|---|---|---|
| | Current density (A $m^{-2}$) | Voltage (V) | Acid conc. (mol $l^{-1}$) | Base conc. (mol $l^{-1}$) | $N_{tr}$ | $A_m$ | Process configuration |
| Mier et al. [31] | 250–1000 | – | 0.05–1.5 | 0.05–2.0 | 1–4 | 0.01 | CL |
| Gineste et al. [33] | 1000 | – | 0.1–5.8 | 0.1–5.7 | 1 | 0.004 | CL |
| Koter and Warszawski [32] | 250–1250 | – | 0.1–1.4 | 0.1–1.6 | 1 | 0.0049 | CL |
| Leon et al. [30] | – | 5 | 0.05–0.08 | 0.05–0.08 | 5 | 0.028 | CL |
| Culcasi et al. [28] | 200 | – | 0.1–0.8 | 0.1–0.8 | 5 | 0.01 | CL |
| Present model | 200–500 | 30–50 | 0.05–1 | 0.05–1 | 40 | 0.16 | F&B, CL |

CL: closed-loop, F&B: feed and bleed.

concentrations, up to 1–1.5 mol $L^{-1}$. At higher concentrations the Nernst potential across the membranes can be significant, leading to high energy consumption. In addition, high current densities cause high ohmic losses and the transport of water inside the BPM can become detrimental. Membrane manufacturers often suggest using a current density sufficiently lower than 1000 A $m^{-2}$. All these aspects must be considered to scale-up the EDBM technology and make it an effective and competitive way of producing chemicals in-situ.

This work aims to develop a model capable of predicting the behaviour of large scale EDBM units across various process configurations and under different operating conditions, relevant for industrial applications. To this end the model simulates an internal staging configuration [19] which is of interest for large membrane area stacks, ensuring high performance and cost-effectiveness. The model adopts the multi-scale approach developed by Culcasi et al. [28] which is comprehensive in describing all the main phenomena occurring within the EDBM unit. The model was modified to extend it to a more complex stack configuration and validated experimentally using data specifically collected from an EDBM pilot plant (19.2 $m^2$ of total membrane area). A sensitivity analysis and economic evaluation, using the continuous feed and bleed configuration, were conducted to demonstrate the potential of the EDBM process. Moreover, as an example of possible scale-up application of the model, it was employed to simulate a double-stage EDBM unit operated in feed and bleed mode.

The paper is organised as follows: Section 2 describes the EDBM equipment simulated by the model and used for its validation, the process configurations investigated during the validation and modelling phases, as well as the key performance indicators analysed. Section 3 presents the multi-scale and economic model utilized in this work, detailing the modifications made to simulate an internal staging configuration, and describes the experimental campaign conducted to validate the model. Section 4 presents electrical profiles along the entire EDBM unit and a preliminary techno-economic analysis conducted in feed and bleed mode to show EDBM potentials. Finally, Section 5 provides the conclusions and future perspectives.

## 2. A description of the EDBM unit

### 2.1. EDBM stack components and configuration

The EDBM unit adopted to conduct the experiments is an FT-ED 1600-3-40-2 purchased from FuMA-Tech GmbH (Germany). A total of 40 triplets, arranged in two cell packs, allow the unit to reach a total membrane area of 19.2 $m^2$. The membranes installed in the EDBM stack are FUMASEP® FAB-PK as anion-exchange membrane, FUMASEP® FKB-PK as cation-exchange membrane, FUMASEP® FBM-PK as bipolar membranes and FUMASEP® F-10150-PTFE as end-membrane. The active membrane area is 0.16 $m^2$ (0.345 m length and 0.454 m width). Additional information about the ion-exchange membranes and spacers adopted in the EDBM stack is reported in Table S1. The electrodes installed in the EDBM stack are dimensionally stable anode (DSA®) and stainless steel (AISI 304) as anode and cathode, respectively. The flow of the solutions through the stack is co-current. Spacers are made from polypropylene, with a thickness of 350 μm. The number of holes in each spacer is equal to 6 with an equivalent diameter of 14.5 mm. The two cell packs installed in the EDBM stack work hydraulically in series with a common manifold which acts as a collector for the first cell pack and as a distributor for the second cell pack. Specifically, the solutions enter the

stack from the bottom left side, flow through the first cell pack, and are then directed to the second cell pack via a linking manifold, finally exiting from the bottom right side of the stack. A schematic representation of the EDBM stack is reported in Fig. 1b. Both cell packs are subjected to the same electric potential difference, utilizing a shared anode (i.e., the positive electrode) and two distinct cathodes (i.e., the negative electrodes). This stack configuration is known as internal staging with two pairs of electrodes of which one electrode is shared (i.e., the anode). This electrode configuration decreases the stack capital cost reducing the amount of material required for the most expensive electrode, i.e., the anode, with respect to the adoption of two different stacks in series. The total current from the DC drive is divided between the two cell packs based on their resistances directing a larger current fraction to the cell pack with a lower electric resistance.

### 2.2. EDBM plant process configuration

The most widely adopted process configurations for the EDBM process are the closed-loop [36,37] and the 'feed and bleed' [25,38]. These two configurations have been selected to validate the model along with operating conditions of interest for industrial applications, both in terms of target concentration of chemicals and current density. This section describes the main characteristics of these process configurations.

#### 2.2.1. Closed-loop configuration

The closed-loop configuration, also known as batch mode, represents the simplest way to reach a certain target concentration of chemicals. Each solution is continuously withdrawn from its tank, passes through the stack to accomplish a certain degree of conversion, and then returns to the tank. In this way the concentration of acid and base in the respective tanks increases over time while the salt concentration in the salt tank decreases. This configuration is a discontinuous operating mode because a certain time is needed to reach a certain target concentration of chemicals. Moreover, the process time is highly dependent on the solutions volumes and on the current density applied to the stack. A schematic representation of the closed-loop configuration is given in Fig. 2a.

#### 2.2.2. Feed and bleed configuration

The feed and bleed configuration extends the residence time of the solutions within the system by recirculating a portion of the stack outlet flow rate back to its inlet. This continuous operating mode can achieve a specific target concentration at the outlet of the stack, starting from water (demineralised water or reverse osmosis permeate), by adjusting the recirculated flow fraction. In a previous paper [27] the feed and bleed configuration was adopted only for acid and base line. Here, instead, also the salt line was operated in feed and bleed mode to prevent the progressive depletion of the salt at the stack inlet guaranteeing steady operation over time. For this reason, an additional tank is used to collect the outlet salt stream from the EDBM unit. This solution might be further treated producing fresh water, then needed again for chemicals generation. A schematic representation of the feed and bleed configuration is shown in Fig. 2b.

### 2.3. Key performance indicators

To assess the performance of the EDBM unit under various operating conditions three main key performance indicators (KPIs) are typically used: current efficiency, specific energy consumption, and specific productivity.

For the continuous feed and bleed process configurations, these indicators are defined as follows:

Current efficiency (CE), often referred as current utilization, is expressed as a percentage. It represents the fraction of the total current supplied to the stack that is converted into the desired product, i.e., acid or base.

$$CE = \frac{\left(Q_{p,out}\, C_{p,out} - Q_{p,in}\, C_{p,in}\right) F}{60\, N_{tr}\, i\, A_m} 100 \tag{1}$$

where subscript $p$ refers to product, i.e., acid or base, subscripts *in* and *out* indicate inlet and outlet streams from the system, $Q$ is the flowrate in L min$^{-1}$, $C$ is the outlet concentration in mol L$^{-1}$ of the product $p$, $F$ is the Faraday constant, i.e., 96,485C mol$^{-1}$, $N_{tr}$ represents the number of triplets installed in the stack, $i$ is the current density in A m$^{-2}$, $A_m$ represents the active membrane area in m$^{-2}$.

Specific Energy Consumption (SEC), expressed in kWh kg$^{-1}$, indicates the energy that must be supplied to the system to produce 1 kg of desired product, i.e., the acid or base.

$$SEC = \frac{U_{ext}\, i\, 2\, A_m}{60\left(Q_{p,out}\, C_{p,out} - Q_{p,in}\, C_{p,in}\right) PM_p} \tag{2}$$

where $U_{ext}$ is the voltage in V supplied to each cell pack of the stack, the factor 2 accounts for the two cell packs considered in this study and $PM_p$ is the molecular weight in g mol$^{-1}$ of the product $p$.

Specific Productivity (SP), expressed in ton y$^{-1}$ m$^{-2}$, provides the tons of chemicals, i.e., acid or base, produced in a working year (8000 h) per unit of total membrane area installed in the EDBM stack.

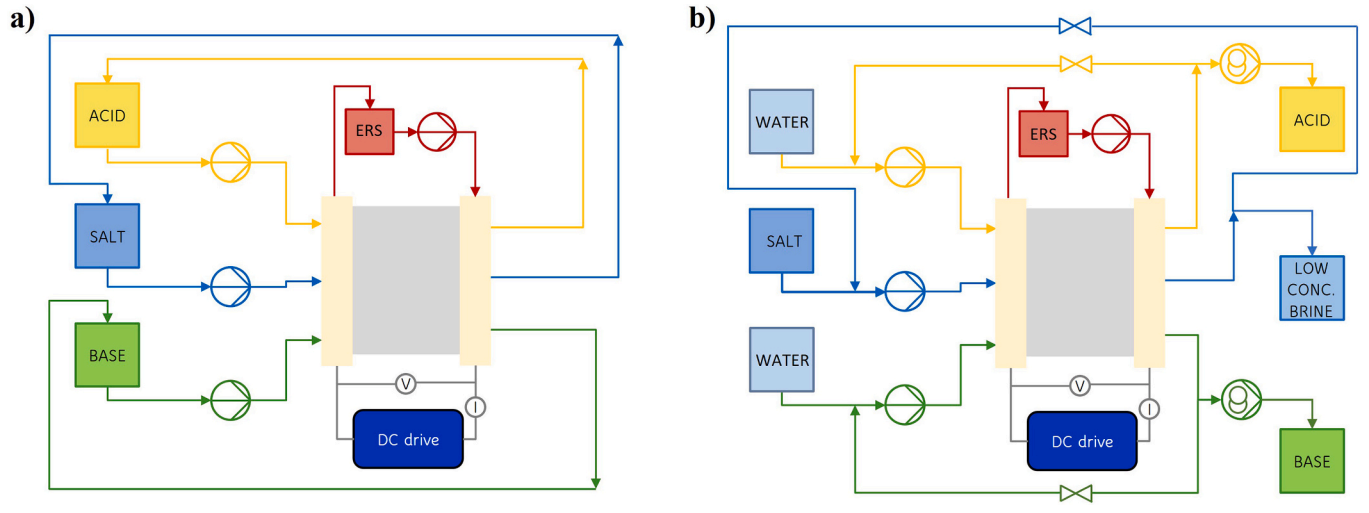


**Fig. 2.** Schematic representation of the process configurations adopted in the EDBM pilot plant: a) closed-loop configuration (discontinuous operating mode); b) feed and bleed configuration (continuous operating mode).

$$SP = \frac{0.48\ \left(Q_{p,out}\ C_{p,out} - Q_{p,in}\ C_{p,in}\right)\ PM_p}{3\ A_m\ N_{tr}} = \frac{0.096\ PM_p\ CE\ i}{F} \quad (3)$$

The $C_{p,in}$ in the above equations was considered equal to zero due to the use of reverse osmosis (RO) permeate (in fact, a dilute NaCl solution at ~400 μS $cm^{-1}$) in the acid and base compartment.

## 3. Model description

### 3.1. Description of the multi-scale model

The model developed in this study adopts a multi-scale modelling approach with distributed parameters to simulate the three-chamber EDBM configuration. This configuration is widely adopted for the simultaneous production of chemicals. The model comprises six different sub-models that span five different levels, from the channel/membrane level up to the external circuit level. The solutions channels are discretized into 50 domain intervals along the flow direction to eliminate grid dependence issues. However, no discretization is applied in the crossflow direction (i.e., perpendicular to the membrane surface). Concentrations gradients, for each discretization domain interval, between the bulk and the membrane/solution interfaces are estimated using polarization coefficients [39]. The multi-scale approach used in this study to simulate EDBM has been previously presented [28]. In this work, the approach is extended to simulate a more intricate EDBM stack configuration, specifically with internal staging, which is of significant interest for industrial applications. The structure of the model used in this study is depicted in Fig. 3.

Except for the highest level (i.e., the external circuit model), all other sub-models simulate steady-state operations. The highest model level computes dynamic mass balances in the solutions tanks, accounting for the dynamic behaviour of the EDBM process in closed-loop mode.

A suitable software tool, gPROMS Model Builder®, is utilized to integrate and solve all the sub-models. For the sake of brevity the full model is described in the Supplementary material file only, while the following sections present a short description of each model level, with more details on the levels that are more relevant to the modifications made to extend the previous model to the new simulation scenario.

#### 3.1.1. Level 1

This level is composed of two different sub-models: the channel model and the bipolar membrane model. The former evaluates solutions chemical-physical properties, while the latter estimates the limiting current density and ion fluxes through the bipolar membrane.

*3.1.1.1. The channel model.* The channel model evaluates the chemical-physical properties of the solutions, such as electrical conductivity, mass density, viscosity, activity coefficients and ion diffusivity in solution using models from the literature or empirical equations. Sherwood numbers are determined using correlations derived from Computational Fluid Dynamics (CFD) simulations. Further details can be found in [39].

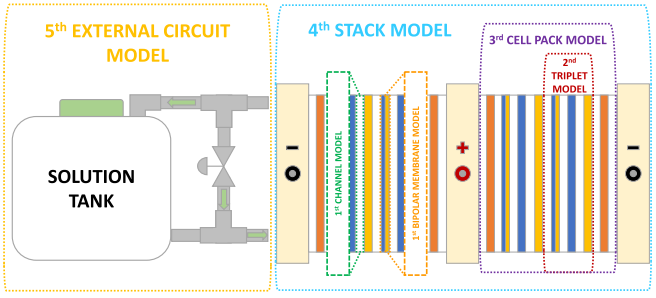


**Fig. 3.** Graphical representation of the multi-scale model structure. Hierarchical levels of the 6 sub-models are represented with the dotted-line areas.

The main modification at this level is the use of the model by McCleskey et al. [40] to determine the conductivities of multi-ion solutions.

*3.1.1.2. The bipolar membrane model.* The bipolar membrane model describes the behaviour of the key element of the EDBM process, the bipolar membrane. The approach developed by Strathmann [41] is employed to estimate the limiting current density and ion fluxes through the two layers of the bipolar membrane. The limiting current density represents the current density at which all salt ions are removed from the transition region. This value is obtained computing a mass balance in the transition region and it is then employed in the estimation of the ion migrative fluxes.

#### 3.1.2. Level 2: the triplet model

The triplet model simulates the behaviour of the repetitive unit of the EDBM process. At this level mass balances are computed in each channel, the electrical potential generated across each triplet is evaluated through the Nernst equation, and, finally, the electrical resistance of the entire triplet is estimated as the sum of the membranes resistances and solutions resistances in the direction perpendicular to the flow of the solutions.

The inputs to this model are membrane and spacer properties. For parameters like thickness, water permeability, and fixed charge density, values previously published in [28] are utilized. While the main features of the spacers, such as thickness as well as porosity in the flow direction and in the plan view, were obtained from the manufacturer. These values are summarized in Table S3. Values for membranes resistance and diffusivity coefficients are obtained from the calibration of the model and they are described in Section 3.3.2.

#### 3.1.3. Level 3: the cell pack model

The cell pack model simulates a certain number of triplets connected hydraulically in parallel. The equivalent hydraulic circuit, for all the solutions, is solved computing mass balances between the channels and the manifolds and assuming a negligible variation in the mass density inside the stack.

#### 3.1.4. Level 4: the stack model

The stack model calculates the solutions resistances in the manifolds and channels and provides the voltage and current profiles along all the triplets installed in EDBM stack. The voltage profile is used to calculate the voltage applied to the stack. Instead, the current profile is employed to compute the percentage of unused current due to the parasitic currents effect (described in Section 1). The equivalent electrical circuit of the EDBM stack was obtained considering the main features of the internal staging configuration (i.e., a unique manifold and a shared anode between the two cell packs). Fig. 4 shows a schematic representation of the equivalent electrical circuit of the stack where only two triplets per cell pack are reported for the sake of simplicity.

Each triplet is modelled as a voltage source and an electrical resistance in the direction perpendicular to the membranes. Instead, two longitudinal resistances are assumed in the flow direction. All these electric components are evaluated in the triplet model.

The resistance related to the connection manifolds between two consecutive channels are evaluated through the following equation:

$$R_{m_i,l,k} = \frac{l_{m_i,k}}{N_{holes}\ S\ \sigma_{m_i,l,k}} \quad (4)$$

where $R$ is the solution resistance in the manifold $m_i$ (i.e., $m_1$ or $m_2$) of the line $l$ (i.e., $a$, $b$ or $s$), in position $k$ (between 1 and $N_{tr}$-1, where $N_{tr}$ is the total number of triplets in the stack); $l_{m_i,k}$ is the length of the manifold $m_i$ in position $k$, $S$ is the section of the manifold, $\sigma_{l,k}$ is the conductivity of the solution $l$ in position $k$, $N_{holes}$ is the number of holes in the spacers. It should be noted that each of these resistances represents the equivalent resistance of parallel resistances, equal to the number of

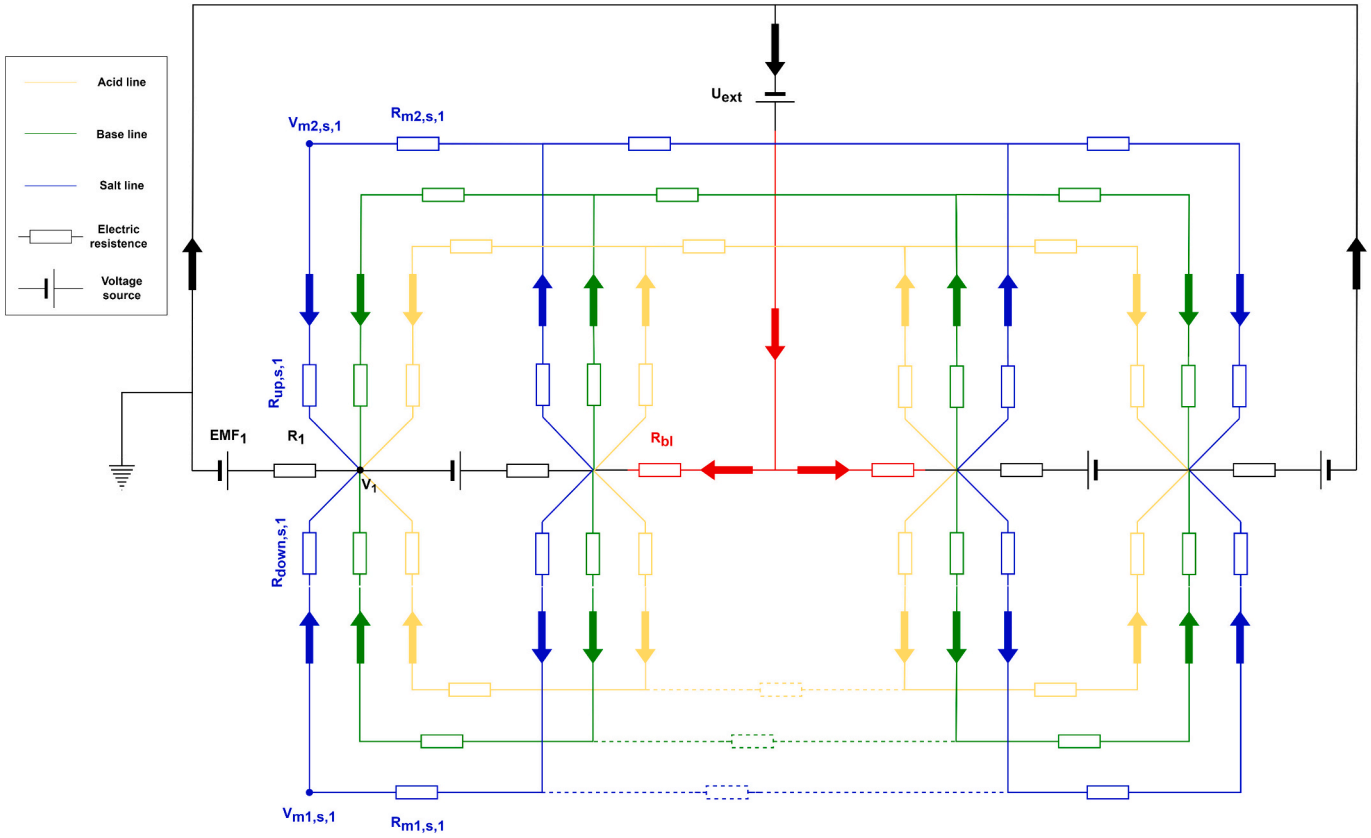


**Fig. 4.** Representation of the equivalent electrical circuit of the EDBM stack, adopting an internal staging configuration with a shared anode. For the sake of clarity, only two repetitive units were represented in each cell pack. $R_{bl}$ represent a lumped parameter known as blank resistance and his meaning and values are described in section supplementary material. Dotted lines represent the interruption in manifold 1, allowing the cell packs to work in series.

holes in the spacers.

The electrode compartments are represented using a lumped parameter known as blank resistance. This parameter accounts for: i) standard electrical potentials, ii) over-voltages of the redox reactions occurring at the electrodes, and iii) the ohmic voltage drops due to the two end-membranes (CEMs), the two electrode compartment channels and the additional acid channel installed to better separate the cell packs from the electrodes chambers (see Fig. S2a). The blank resistance was obtained performing a laboratory test described supplementary material. The DC drive that powers the system is represented as an electrical generator.

The hydraulic connections between the two cell packs can be electrically modelled as additional branches of the electric circuit with an electric resistance. The presence of this electric branches determines the onset of additional parasitic ionic pathways. The cell packs share a central common anode (positive electrode), while two distinct cathodes (negative electrodes) are positioned at the two extremes of the stack. The voltage for both cathodes is considered to be zero (i.e., the ground potential).

This model simulates two manifolds: the lower (designated as 1) and the upper (designated as 2). According to the scheme in Fig. 4, an interruption is placed in the anode position of manifold 1, with the two cell packs only connected through manifold 2. This interruption in the manifold 1 is simulated by setting the $R_{m_1,l,N_1}$ to $10^8$ Ω for all three solutions (where $N_1$ is the number of triplets in the first cell pack). The resistance of manifold 2 denoted as $R_{m_2,l,N}$, is derived for the three solutions using Eq. (4), where length of the linking manifold section connecting the two cell packs, $l_{m_2,N_1}$, is fixed to 6 cm. This difference in length is due to the presence of the anodic chamber between the cell packs. Due to this different length, this resistance is about two orders of magnitude greater than the other manifolds resistances.

Kirchhoff's and Ohm's laws are applied to the nodes and branches of the equivalent electrical circuit, respectively, to obtain the current and voltage profiles along the entire stack.

For the first cell pack the following equation are employed:

$$I_{m_i,l,1} = \left(V_{m_i,l,2} - V_{m_i,l,1}\right)/R_{m_i,l,1} \tag{5}$$

where $I_{m_i,l,1}$ is the current flowing in the manifold $m_i$ of the line $l$, in position 1 and $V_{m_i,l,k}$ is the voltage in the manifold $m_i$ of the line $l$, in position $k$,

$$I_{up,l,1} = \left(V_{m_2,l,1} - V_1\right)/R_{up,l,1} \tag{6}$$

$$I_{down,l,1} = \left(V_{m_1,l,1} - V_1\right)/R_{down,l,1} \tag{7}$$

where $I_{x,l,1}$ is the current flowing in the $x$ (i.e., *up*, *down*) part of the channel of the line $l$, in position 1, $R_{x,l,1}$ is the resistance of $x$ (i.e., *up*, *down*) part of the channel of the line $l$, in position 1 and $V_1$ is the voltage of the stack in position 1 (see Fig. 4).

$$V_1 = I_1 R_{av,1}/A_m + E_{av,1} \tag{8}$$

where $I_1$ is the current flowing between $V_1$ and the left cathode, $E_{av,1}$ and $R_{av,1}$ are the average triplet membrane potential and the average cell resistance of the cell in position 1, respectively.

$$I_{k-1} = I_k + \sum\nolimits_l \left(I_{up,l,k-1} + I_{down,l,k-1}\right) \tag{9}$$

$$I_{m_1,l,k-1} = I_{down,l,k} + I_{m_1,l,k} \tag{10}$$

$$I_{m_2,l,k-1} = I_{up,l,k} + I_{m_2,l,k} \tag{11}$$

$$I_{m_i,l,k} = \left(V_{m_i,l,k+1} - V_{m_i,l,k}\right)/R_{m_i,l,k} \quad (12)$$

$$I_{up,l,k} = \left(V_{m_2,l,k} - V_k\right)/R_{up,l,k} \quad (13)$$

$$I_{down,l,k} = \left(V_{m_1,l,k} - V_k\right)/R_{down,l,k} \quad (14)$$

$$V_k = V_{k-1} + I_k R_{av,k}/A_m + E_{av,k} \quad (15)$$

The validity interval of equations between Eqs. (9) and (15) is for **k** [2 to $N_1$], where $N_1$ is the number of triplets installed in the first cell pack.

For the second cell pack the following equation are used:

$$I_{k+2} = I_{k+1} + \sum\nolimits_l \left(I_{up,l,k} + I_{down,l,k}\right) \quad (16)$$

$$I_{m_1,l,k-1} = I_{down,l,k} + I_{m_1,l,k} \quad (17)$$

$$I_{m_2,l,k-1} = I_{up,l,k} + I_{m_2,l,k} \quad (18)$$

$$I_{m_i,l,k} = \left(V_{m_i,l,k+1} - V_{m_i,l,k}\right)/R_{m_i,l,k} \quad (19)$$

$$I_{up,l,k} = \left(V_{m_2,l,k} - V_{k+1}\right)/R_{up,l,k} \quad (20)$$

$$I_{down,l,k} = \left(V_{m_1,l,k} - V_{k+1}\right)/R_{down,l,k} \quad (21)$$

$$V_{k+1} = V_{k+2} + I_{k+2} R_{av,k}/A_m + E_{av,k} \quad (22)$$

The validity interval of equations between Eqs. (16) and (22) is for **k** [$N_1 + 1$ to $N_{tr}$-1].

$$I_{N_{tr}+2} = I_{N_{tr}+1} + \sum\nolimits_l \left(I_{up,l,N_{tr}} + I_{down,l,N_{tr}}\right) \quad (23)$$

$$I_{m_1,l,N_{tr}-1} = -I_{down,l,N_{tr}} \quad (24)$$

$$I_{m_2,l,N_{tr}-1} = -I_{up,l,N_{tr}} \quad (25)$$

$$V_{m_1,l,N_{tr}} - V_{N_{tr}+1} = I_{down,l,N_{tr}}\ R_{down,l,N_{tr}} \quad (26)$$

$$V_{m_2,l,N_{tr}} - V_{N_{tr}+1} = I_{up,l,N_{tr}}\ R_{up,l,N_{tr}} \quad (27)$$

$$V_{N_{tr}+1} = I_{N_{tr}+2} R_{av,N_{tr}}/A_m + E_{av,N_{tr}} \quad (28)$$

In the anode position, to connect the two cell packs, the following equation are applied:

$$V_{N_1+1} = U_{ext} \quad (29)$$

$$I_{N_1+1} + I_{N_1+2} = I_{ext} \quad (30)$$

$$I_1 + I_{N_1+2} = I_{ext} \quad (31)$$

$$U_{ext} = R_U\ I_{ext} \quad (32)$$

$$V_{N_1+1} = V_{N_1} + I_{N_1+1}\ R_{bl}/A_m \quad (33)$$

$$V_{N_1+1} = V_{N_1+2} + I_{N_1+2}\ R_{bl}/A_m \quad (34)$$

where $U_{ext}$ and $I_{ext}$ are the external voltage and current supplied by the Dc drive and $R_U$ is the apparent electrical resistance of the entire stack.

Once current and voltage profile (i.e., I and V) along the entire stack were determined two key metrics are computed: the percentage of unused current due to parasitic effects and the external voltage applied to the stack.

The percentage of unused current due to parasitic currents effects is calculated using the following equation:

$$\eta_I = \frac{A_m\ i - \frac{1}{2}\left(\frac{1}{N_1}\sum_{j=1}^{N_1} I_j + \frac{1}{N_2}\sum_{j=N_1+2}^{N_{tr}+2} I_j\right)}{A_m\ i}\ 100 \quad (35)$$

where $N_2$ is the number of triplets in the second cell pack.

The voltage applied to the stack is equal to the voltage in the anode position which represents the maximum value observed across the stack.

#### 3.1.5. Level 5: the external hydraulic circuit model

At the highest hierarchical model level, the elements constituting the external hydraulic circuit, including solution tanks, recirculating loops and hydraulic nodes, are simulated. This level differs depending on the process configuration adopted, i.e., closed-loop or feed and bleed.

For the closed-loop configuration, only the solution tanks for acid, base and salt are simulated. Dynamic mass balances are computed, assuming perfect mixing of the solutions. It is noteworthy that the dynamic equations implemented at this level do not make the model fully dynamic as all the other levels simulate steady-state conditions. However, the model can simulate dynamic process configurations, such as the closed-loop, as the dominant dynamic of the system (i.e., the tanks) is simulated.

The feed and bleed configuration is a continuous operating mode and no dynamic equations are implemented. In this case, the recirculation loop from the outlet back to the stack inlet is simulated to increase the residence time of the solution inside the stack. Two hydraulic nodes, for each solution, connecting the recirculating loop to the main flow stream are simulated. Here steady-state mass balances are computed.

### 3.2. Economic model

The economic model evaluates the competitiveness of the EDBM process to produce sodium hydroxide, which results the more profitable product. To this end the levelized cost of sodium hydroxide (LcoNaOH) is estimated. The LcoNaOH, expressed in € $ton^{-1}$, represents the minimum sale price of the produced NaOH to guarantee a net present value (NPV) equal to zero at the end of the project life. The model considers all the major components of both capital and operating expenditures. Moreover, the compound interest calculation is applied in determining the LcoNaOH. Several parameters are employed as model inputs: stack features, capital costs and economic parameters. All the parameters are described in Table 2.

The triplet cost (US$ $m^{-2}$) is estimated through the following equation:

**Table 2**
Input parameters of the economic model.

| | Symbol | Unit | Value | Reference |
|---|---|---|---|---|
| *Stack parameter* | | | | |
| Active membrane area | $A_m$ | $m^2$ | 0.16 | – |
| Number of triplets in the stack | $N_{tr}$ | – | 40 | – |
| Number of stacks in series | $N_S$ | – | 1–2 | – |
| *Capital costs* | | | | |
| BPM cost | $BPM_{cost}$ | US$ $m^{-2}$ | 300 | |
| AEM/CEM cost | $MPM_{cost}$ | US$ $m^{-2}$ | 135 | [42] |
| Spacer cost | $S_{cost}$ | US$ $m^{-2}$ | 10 | |
| *Economic parameters* | | | | |
| US$/€ conversion | $C_{conv}$ | € $US\$^{-1}$ | 0.915 | [43] |
| Electricity price | $E_p$ | € $kWh^{-1}$ | 0.1 | [44] |
| Discount rate | j | % | 5 | [28] |
| Membrane and spacers lifetime | $M_{lt}$ | y | 5 | [45] |
| Peripherals and electrodes lifetime | $PE_{lt}$ | y | 10 | |
| Project lifetime | $P_{lt}$ | y | 10 | |
| *Performance indicators*[a] | | | | |
| Specific energy consumption | SEC | kWh $kg^{-1}$ | | |
| Specific productivity | SP | ton $y^{-1}$ $m^{-2}$ | | |

[a] Inputs to the economic model obtained from the multi-scale model.

$$T_{cost} = BPM_{cost} + 2\,MPM_{cost} + 3\,S_{cost} \quad (36)$$

where $BPM_{cost}$ and $MPM_{cost}$ are the cost of bipolar and monopolar membranes respectively and $S_{cost}$ is the spacers cost. A triplet cost of 600 US$ $m^{-2}$ is obtained as a reference value.

The cost of the cell packs installed in the stack (€) is calculated as follows:

$$IM_{cost} = T_{cost} C_{conv} N_{tr} A_m \quad (37)$$

where $C_{conv}$ coverts from US$ to €. The electrodes and plates and frames cost can be obtained as a function of the cell packs cost [42].

$$EPF_{cost} = 0.5\,IM_{cost} \quad (38)$$

The total cost of the stack, in €, can be written as:

$$TS_{cost} = IM_{cost} + EPF_{cost} \quad (39)$$

The cost relative to peripheral equipment (i.e., pumps, DC drive, electrical cabinet, monitoring instrumentation and control systems) can be estimated through the following equation:

$$PE_{cost} = 1.2\,TS_{cost}(1 + 0.3(N_s - 1)) \quad (40)$$

where $N_s$ is the number of stacks in series. Consequently, adding a second stack in series increases the cost of associated with the peripheral equipment of 30 %, since some of them are already installed or should only be increased in size.

The initial capital investment (ICI) at the start of the project life is given by:

$$ICI = TS_{cost} N_s + PE_{cost} \quad (41)$$

Often the lifetime of the membranes and spacers $M_{lt}$ is lower than the project lifetime $P_{lt}$. Subsequently a replacement of the cell packs in necessary at the end of $M_{lt}$.

Maintenance cost ($Maint_{cost}$) and the Total Energy Consumption (TEC) are considered as operating costs of the EDBM plant. Maintenance cost (€ $y^{-1}$) are estimated as follows [42]:

$$Maint_{cost} = 0.1\,ICI \quad (42)$$

The total energy consumption (€ $ton^{-1}$) is calculated using the following equation:

$$TEC = 1.1\,SEC\,E_p 10^3 \quad (43)$$

where $E_p$ is the electricity price, the factor 1.1 accounts for the electrical consumption of the EDBM stack and the peripheral equipment (calculated as 10 % of the stack energy consumption [42]), $10^3$ coverts the units from € $kg^{-1}$ to € $ton^{-1}$. The Process Capacity (PC), expressed in ton $y^{-1}$, is calculated as follows:

$$PC = SP\,N_{tr} A_m \quad (44)$$

The LcoNaOH is calculated using the following equation:

$$LCoNaOH = \frac{Maint_{cost}}{PC} + TEC + \frac{ICI(1+j)^{P_{lt}} + IM_{cost} N_s (1+j)^{M_{lt}}}{PC \sum_{y=1}^{P_{lt}} (1+j)^{(P_{lt}-y)}} \quad (45)$$

where $j$ is the discount rate.

### 3.3. Model calibration and validation

#### 3.3.1. Experimental test in feed and bleed mode

The feed and bleed configuration is a continuous operating mode, and four different steady-state conditions were investigated in a single operating day. The four conditions differ in the current-density adopted (i.e., 200 or 400 A $m^{-2}$) and chemicals concentrations (i.e., in the range of 0.5–1 mol $L^{-1}$). In Table 3, the operating conditions adopted for each steady-state are reported.

For the test a volume of 500 L of synthetic salt solution at a concentration of 1 mol $L^{-1}$ was prepared mixing RO permeate (~ 400 μS $cm^{-1}$) and high-grade NaCl (>99.5 % purity, Saline di Volterra S.r.l). As electrode rinse solution, a sodium sulphate solution at 0.25 mol $L^{-1}$ was used. A volume of 125 L of ERS was prepared using RO permeate (~ 400 μS $cm^{-1}$) and technical grade $Na_2SO_4$ (CR GRUPO CRIMIDESA). Acid and base inlet tanks were also filled with RO permeate, since the impact of elevated stack resistance at the beginning of the test can neglected in feed & bleed operating mode, thanks to the recirculation loop within the system, which mixes a part of the stack outlet solution back into the inlet. As a result, the conductivity of the solutions entering the stack is increased for the acid and base streams, and slightly decreased for the salt stream. During the test acid and base samples (50 mL) were collected for analytical characterization. Titrations were performed for the acid and base solutions using $Na_2CO_3$ (0.05 mol $L^{-1}$) and HCl (0.1 mol $L^{-1}$), respectively, adopting methyl orange as an indicator. Regarding the salt solution, only the conductivity was measured. Voltage and current values were read from the display of the DC drive (AF02 Giussani S.r.l.). The voltage value was periodically checked with a multimeter (Fluke 8808 A).

The results of the tests conducted are reported in Fig. 5. Apart from the initial transitory phase, a stable trend is observed for the monitored variables (acid and base concentrations and voltage) over time. After each steady-state condition had been reached, three samples were collected (every 10 min).

It can be noted that the steady-state conditions at the two different current densities are perfectly proportional in terms of outlet flow rates. For instance, when the current density is doubled, the outlet flow rate for the three main solutions also doubles.

#### 3.3.2. Model calibration

The model was calibrated with the experimental test in feed and bleed mode to increase its predictive accuracy, accounting for non-ideal phenomena occurring in the EDBM unit, such as internal leakages, pressure differences between channels, membrane deformation and fouling. But also, to account for uncertainties in some membrane properties, such as membrane ion diffusivities and electric resistances.

The parameters used for calibration are: i) an additional term in the Nernst-Planck equation, which accounts for the non-ideal phenomena mentioned above, ii) ion-diffusivities in the membranes, iii) a correction factor for the cell packs resistance.

The Nernst-Planck flux equation is a widely used approach to describe the transport of ions in ion-exchange membranes. Specifically, the ion transport is given by the sum of two contributions: a diffusion

**Table 3**
Operating conditions adopted in each steady-state condition investigated in feed and bleed mode.

| Steady-state | Current density (A $m^{-2}$) | Outlet acid flowrate (L $min^{-1}$) | Outlet base flowrate (L $min^{-1}$) | Outlet salt flowrate (L $min^{-1}$) | Rec. acid flowrate (L $min^{-1}$) | Rec. base flowrate (L $min^{-1}$) | Rec. salt flowrate (L $min^{-1}$) | ERS flowrate (L $min^{-1}$) |
|---|---|---|---|---|---|---|---|---|
| A | 400 | 2 | 2 | 1.5 | 3 | 3 | 3.5 | 20 |
| B | 400 | 1 | 1 | 1.5 | 4 | 4 | 3.5 | 20 |
| C | 200 | 1 | 1 | 0.75 | 4 | 4 | 4.25 | 20 |
| D | 200 | 0.5 | 0.5 | 0.75 | 4.5 | 4.5 | 4.25 | 20 |

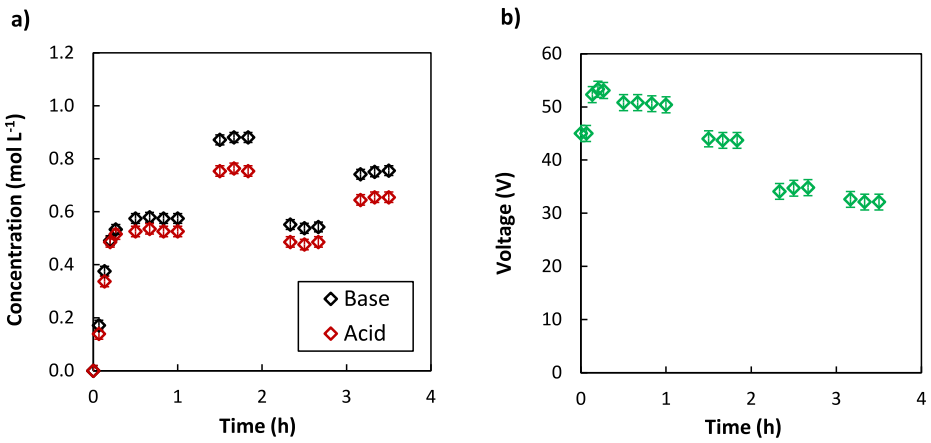


**Fig. 5.** Analysis of stationary operations of the EDBM pilot operated in feed and bleed mode: a) acid and base concentration; b) voltage applied to the stack.

term and a migrative term.

$$J_{i,m} = -\sum_{j} D_{i,j,M} \nabla C_{j,m} + \frac{t_{i,m} i}{z_i F} \tag{46}$$

where $J_{i,m}$ is the total molar flux of the specie $i$ across the generic membrane $m$ (i.e., AEM, CEM or BPM), the sum is extended to all the ionic species, $D_{i,j,m}$ is the cross-diffusion coefficient, $C_{j,m}$ is the concentration of the species $j$ in the membrane phase, $t_{i,m}$ is the transport number of the species $i$ in the membrane at the solution-membrane interface, $z_i$ is the valence of ion $i$.

This equation is derived assuming some standard approximations [46] and consequently its validity is limited to dilute electrolyte solutions.

The modified Nernst-Planck equation adopted in this work is reported here.

$$J_{tot,i,l} = J_{ohm,i,l} + J_{diff,i,l} + J_{cal,i,l} \tag{47}$$

where $J_{tot,i,l}$ is the total flux of the ion $i$ across the two membranes bounding the channel $l$ (acid, base or salt), $J_{ohm,i,l}$ and $J_{diff,i,l}$ are the total ohmic and the total diffusive flux (calculated as described in the supplementary material), respectively and $J_{cal,i,l}$ is the calibration parameter used to correct the Nernst-Plank equation.

There are twelve $J_{cal,i,sol}$ calibration parameters in total, since the ions under consideration are four ($Na^+$, $Cl^-$, $H^+$, $OH^-$) and the solutions are three (i.e., acid, base and salt). However, certain relationships exist among these parameters. One of these is the mass balance equation between the calibration fluxes of the three solutions flowing in an EDBM stack:

$$J_{cal,i,acid} + J_{cal,i,base} + J_{cal,i,salt} = 0 \tag{48}$$

The second relationship is the electroneutrality requirement between the calibration parameters:

$$\sum J_{cal,i,acid} z_i = 0 \tag{49}$$

$$\sum J_{cal,i,base} z_i = 0 \tag{50}$$

where the sum is extended to all the ions. The flux calibration parameters and ion-diffusivities used in the model are reported in Table 4. All the calibration fluxes ranged, in all the cases, from 2 % to 7 % for the main ion of each compartment compared to the total flux of these ions in the channels.

The ion-diffusivities in the membranes were also obtained from the calibration of the model due the difficulty in estimating their values from the experimental tests.

Finally, a correction factor for the cell pack areal resistance is considered because a decrease of the apparent stack areal resistance is observed as a function of the current density at a fixed target concentration of the base solution, Fig. S1. This reduction is attributed to the membrane resistance, which is the predominant resistance of the stack, and the variations of the solutions resistances are considered in the model. The same correction factor for the stack resistance is applied to all the membranes and it is reported as a function of the current density.

$$R_{cal} = 3.7\ 10^{-6}\ i^2 - 4.1\ 10^{-3}\ i + 2.3 \tag{51}$$

The correction factor obtained is then multiplied by the membrane resistance, which in turn is used to evaluate the triplet resistance through the following equation:

$$R = \sum_{l} R_l + \sum_{m} R_{cal} R_m \tag{52}$$

where $R_l$ and $R_m$ are the electrical resistance of the solution channels (i.e., acid, base, and salt) perpendicular to the membranes and the electrical resistance of the membranes (i.e., CEM, AEM, and BPM).

The above calibration procedure resulted into the simulated vs experimental trend illustrated in Fig. 6, where acid and base concentrations as well as the voltage applied to the stack are shown for a feed and bleed operating configuration. The discrepancy between the model results and the experimental values is evaluated, with an average discrepancy of 5 % identified across all variables. In all cases, discrepancy values lower than 11 % are recorded. When comparing this discrepancy will the experimental error (i.e., 4–5 %), the values seem comparable, further confirming the high predictive capability of the

**Table 4**
Calibration parameters adopted in the model to account for non-ideal phenomena such as internal leakages, pressure differences between channel, deformation and fouling of membranes.

| | Acid | Base | Salt |
|---|---|---|---|
| | (mol $m^{-2}$ $s^{-1}$) $10^5$ | | |
| $J_{cal,l,Na}$ | 7 | −13.2 | 6.2 |
| $J_{cal,l,Cl}$ | −14.2 | 8.2 | 5.99 |
| $J_{cal,l,OH}$ | 0.8 | −22.4 | 21.6 |
| $J_{cal,l,H}$ | −20.4 | −1 | 21 |

| | AEM | CEM | AEL | CEL |
|---|---|---|---|---|
| | ($m^2$ $s^{-1}$) $10^{11}$ | | | |
| $D_{Na,m}$ | 3.1 | 1 | 4.1 | 5.7 |
| $D_{Cl,m}$ | 1.6 | 1.6 | 2.2 | 8.5 |
| $D_{OH,m}$ | 9.5 | 7.5 | 6 | 6 |
| $D_{H,m}$ | 7.35 | 7.1 | 2 | 14.6 |

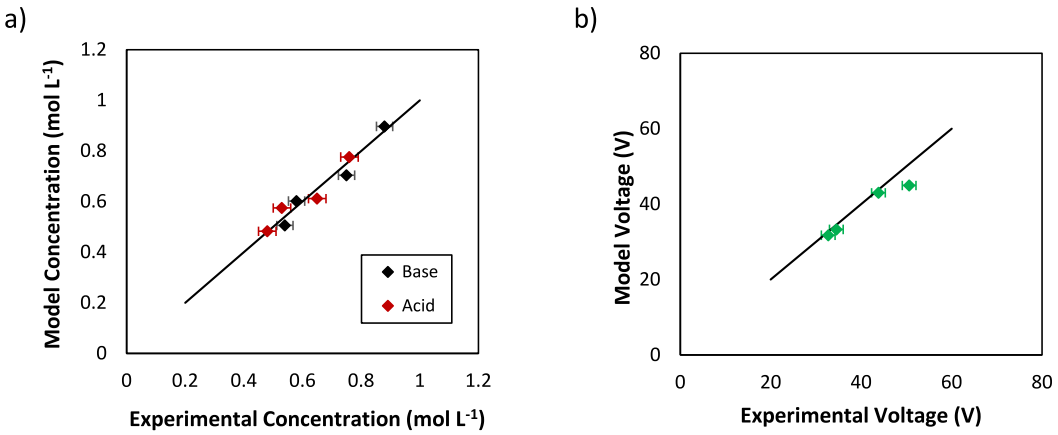


**Fig. 6.** Comparison between experimental and model results in terms of acid and base concentration as well as of voltage applied to the stack.

model.

### 3.3.3. *Experimental tests in closed-loop mode*

The model was tested in closed-loop configuration under different current densities, i.e., 300, 400 and 500 A $m^{-2}$. The range of current density results of practical interest for industrial-scale applications because it reduces the process time needed to covert a certain volume to specific target concentration. As an example, increasing the current density from 200 A $m^{-2}$ to 500 A $m^{-2}$ allow to reduce the process time from 9 h to 4 h for an initial solution volume of 300 L and a target concentration of 1 mol $L^{-1}$ [25].

Details about the operating conditions adopted in each test and the main results are summarized in Table 5. Low concentrated acid and base solutions were employed to preclude excessive stack resistance at the beginning of the test, that otherwise will negatively affect the performance of system. These tests were already published in a previous paper [25].

### 3.3.4. *Closed-loop validation*

To validate the model calibration, the test described in Table 5 were employed. The model was validated under three different process conditions, specifically at current densities of 300, 400 and 500 A $m^{-2}$. The comparison between the model predictions and experimental results is illustrated in Fig. 7. Both chemical concentrations and stack voltage profiles, as functions of time, are presented. The model accurately predicts the concentration profiles, and the applied voltage is also well predicted, except for the initial phase of the test. Table 6 reports both the maximum and average discrepancies for test performed.

At 300 A $m^{-2}$, the maximum discrepancies found for the acid and base profiles are 6.2 % and 2.5 %, respectively. For the voltage profile, a maximum discrepancy of 21 % is observed, but only at the beginning of the voltage profiles when the conditioning of the membranes is not completed. Indeed, before testing the stack was stored in RO permeate (~ 400 μS $cm^{-1}$) and some time is required after the start-up of the test for the initial water to be replaced by the solutions. Predicting this behaviour using traditional modelling tools is challenging, and a certain membrane conditioning time period should be determined experimentally. Increasing the current density to 400 A $m^{-2}$ does not alter the model predictive capability. Indeed, the average discrepancies range between 3.7 % and 8.4 %. As in the previous test, a maximum voltage discrepancy of 20 % is noted at the beginning and can also be attributed to the membranes incomplete conditioning. At 500 A $m^{-2}$, the maximum current density tested, discrepancies remain lower than 10 % apart from the voltage, for which a maximum voltage discrepancy of 26 % is observed at the beginning (due to membranes incomplete conditioning), while on average the discrepancy is 8.4 %. It is worth noting that the average discrepancies found are comparable with the experimental errors observed in the measurement of these variables, typically between 3 and 9 %.

## 4. Results

### 4.1. *Electrical profiles and parasitic currents evaluation for the internal staging configuration*

In this section, the main output of the stack model, i.e., current and voltage profiles, are shown to better understand how the internal staging configuration works. Additionally, the impact of parasitic currents on the stack performance is also evaluated.

Voltage and current profiles as a function of the number of triples are reported in Fig. 8 for a test conducted in feed and bleed mode at 400 A $m^{-2}$ and fixing a target concentration of base of 1 mol $L^{-1}$. An inlet concentration of 1 mol $L^{-1}$ of NaCl is employed for the salt steam, while, for acid and base line, water with a low salt content (1 mmol $L^{-1}$ of NaCl) is utilized.

The total current is supplied from the anode to the cell packs, and it is split inversely proportional to the cell pack resistances. This fact could be observed in the current profile (Fig. 8a) where two red symbols are shown. The current supplied to the second cell pack is slightly higher due to its lower resistance. Along the cell packs, the current displays a minimum around the middle, at triplets 11 and 30 for the first and second cell packs, respectively. Moving from the anode to the cathode,

**Table 5**
Operative conditions adopted and main results of the tests conducted in closed-loop mode.

| | Operative conditions | | | Test 1 | | Test 2 | | Test 3 | |
|---|---|---|---|---|---|---|---|---|---|
| | $Q$ (l/min) | $C_0$ (l/min) | $V_0$ (l) | $C_f$ (l/min) | $V_f$ (l) | $C_f$ (l/min) | $V_f$ (l) | $C_f$ (l/min) | $V_f$ (l) |
| Duration (h) | | | | 7.2 | | 4 | | 4 | |
| i (A $m^{-2}$) | | | | 300 | | 400 | | 500 | |
| Acid | 5 | 0.05 | 300 | 0.905 | 336 | 0.827 | 318 | 0.902 | 329 |
| Base | 5 | 0.05 | 300 | 1.00 | 343 | 0.888 | 328 | 1.00 | 327 |
| Salt | 5 | 1 | 900 | | | | | | |
| ERS | 20 | 0.25 | 125 | | | | | | |

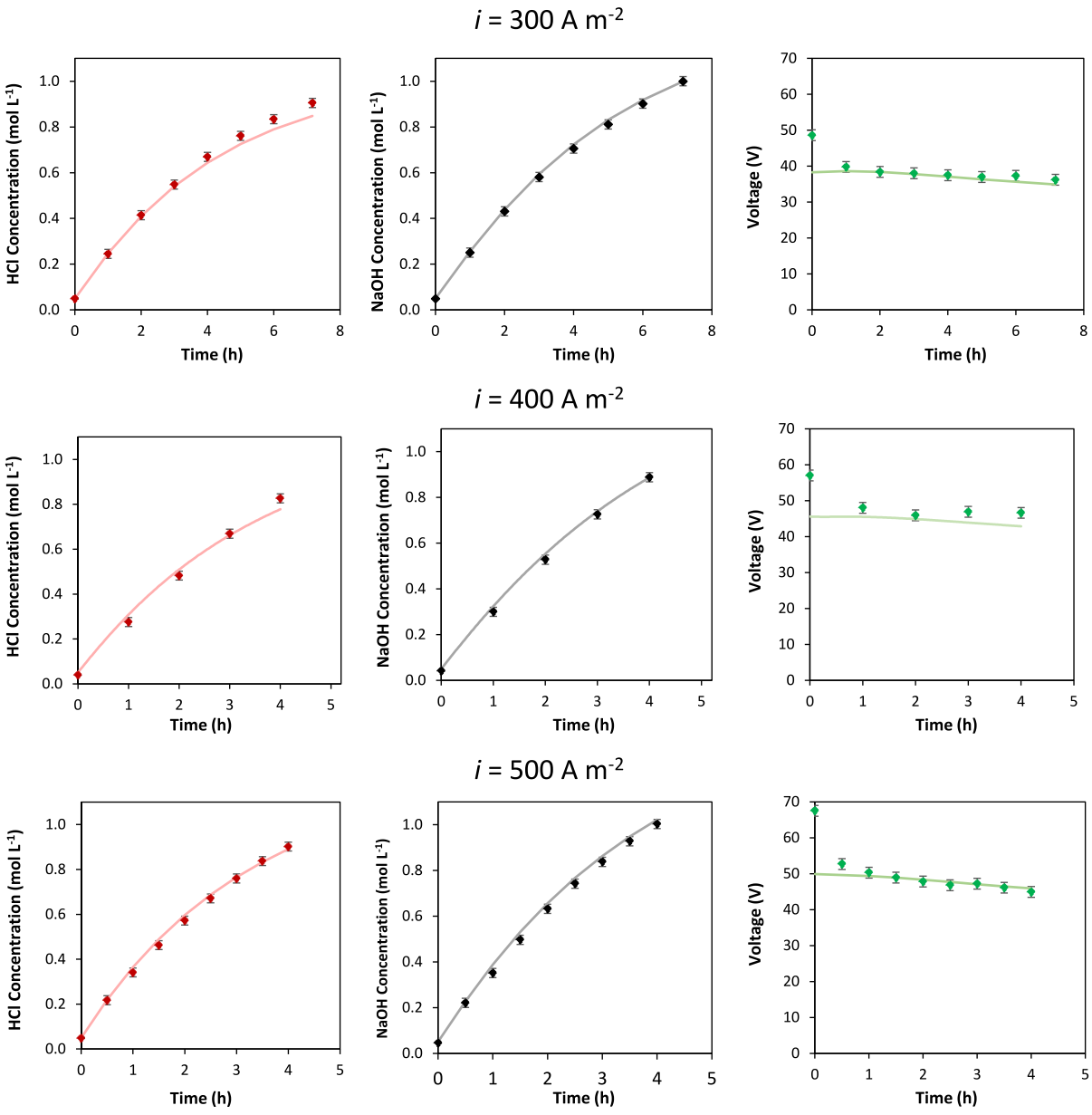


**Fig. 7.** Trends of the main variables of the EDBM process (acid and base concentration as well as voltage applied to the stack) for the three different tests performed in closed-loop mode at constant current densities. Symbols represent experimental results, while the continuous line represents model results.

**Table 6**
Average and maximum deviation between model and experimental results and comparison with the experimental error made in measuring concentrations and voltage.

| | 300 A m$^{-2}$ | | | | 400 A m$^{-2}$ | | | | 500 A m$^{-2}$ | | | |
|---|---|---|---|---|---|---|---|---|---|---|---|---|
| | Discrepancy (%) | | Exp. error (%) | | Discrepancy (%) | | Exp. error (%) | | Discrepancy (%) | | Exp. error (%) | |
| | Average | Max | Average | Max | Average | Max | Average | Max | Average | Max | Average | Max |
| $C_{acid}$ | 3.2 | 6.2 | 3.7 | 8.0 | 6.1 | 8.6 | 6.7 | 9.1 | 3.1 | 7.0 | 3.4 | 6 |
| $C_{base}$ | 1.7 | 2.5 | 3.7 | 8.0 | 3.7 | 8.1 | 6.9 | 9.1 | 5.3 | 11 | 3.3 | 6 |
| $U_{ext}$ | 4.4 | 21 | 3.9 | 4.1 | 8.4 | 20 | 3.4 | 3.5 | 4.3 | 26 | 3.1 | 3.3 |

the current divides in each triplet and a certain portion flows through parasitic paths (manifolds and channels) instead of passing through the active membrane area. The observed minimum in the current profile for each cell pack is correlated to the relative weight of the cell pack resistance and the resistance of the parasitic pathways in each stack position (i.e., in each triplet). At the end of the cell packs (cathode side) the electrical current in the final triplets (i.e, 1 and 40) equals that reaching the cathode. Ultimately, the sum of the currents in the two cathodes is equal to the total current supplied to the stack.

The voltage profile is determined by setting the cathode voltage to zero and evaluating the voltage drop across each triplet of the cell pack and its respective cathode. The trend is symmetric between the two cell packs, with small changes due to the difference in the conductivities of the solutions flowing inside. The red symbol in Fig. 8b represents the

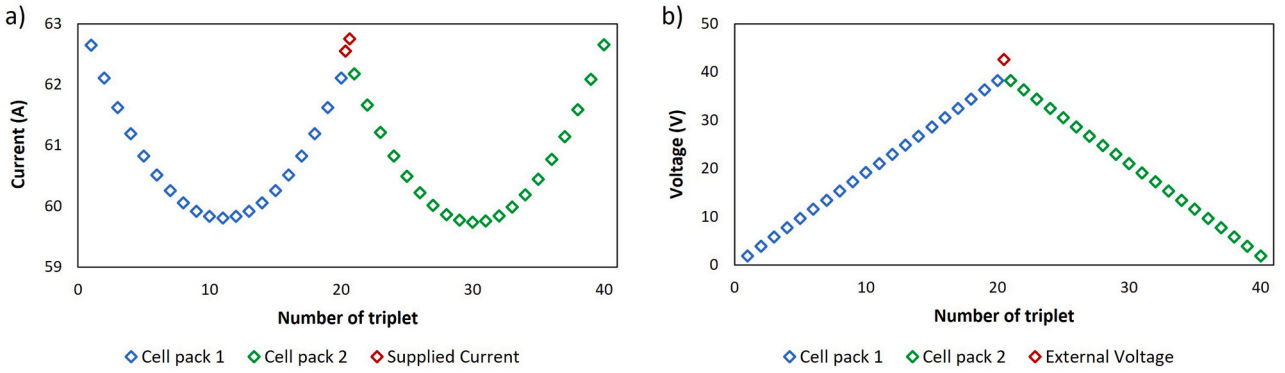


**Fig. 8.** Current and voltage profiles along the entire EDBM stack obtained with the model. The blue and green symbols represent the first and the second cell pack, respectively; the red symbols represent the anode, which supplies the current to both the cell packs. The voltage read at the anode is equal to the external voltage (the voltage in the cathodes is assumed equal to 0). The profiles were obtained at 400 A $m^{-2}$, fixing the target concentration of NaOH to 1 mol $l^{-1}$.

anode voltage, i.e., the external voltage applied to the stack.

For the current profile depicted in Fig. 8 the percentage of unused current due to parasitic currents is evaluated using Eq. (35). This value represents the percentage reduction of the average current utilized by the stack to produce chemicals compared to the total current supplied by the DC drive. A value of 3.1 % is found for the entire stack while at minimum points of the current profile local unused current values of 4.5 % and 4.7 % are found for the first and second cell packs, respectively. These low values result from the small number of triplets present in each cell pack and to the well-designed EDBM stack in terms of channels length and manifolds diameter. Consequently, it can be stated that the internal staging configuration with a shared anode effectively allows for a reduction of the parasitic currents, despite the linking manifold, and minimizes the capital expenditure compared to the use of two separate EDBM stacks in series.

### 4.2. Techno-economic analysis of EDBM potential

In this section, the validated model is used to conduct a sensitivity analysis based on the main process variables and, secondly, an economic evaluation of the Levelized Cost of sodium hydroxide (LcoNaOH). In both cases, the feed and bleed process configuration is used as it is attractive for industrial applications.

The sensitivity analysis investigates the effect of varying current density and target concentration of sodium hydroxide on the key performance indicators of the EDBM process, (described in Section 2.3). The variation range of these operating variables was selected to offer insights pertinent to industrial applications. The target concentration varied between 0.5 and 1 mol $L^{-1}$ aligning with the interests of various applications highlighted in Section 1. The current density, instead, is tested between 320 and 600 A $m^{-2}$, which guarantees high specific productivity (SP), reasonable ohmic loss and safe conditions for the bipolar membranes. Also in this case, an inlet concentration of 1.0 mol $L^{-1}$ of NaCl is employed for the salt steam, while, for acid and base line, water with a low salt content (1 mmol $L^{-1}$ of NaCl) is utilized, emulating an RO permeate. Different target concentrations are obtained by changing the outlet flow rates from the entire EDBM unit while maintaining constant flowrates through the stack (constant channels flow velocities) equal to 5 L $min^{-1}$. The outlet flowrates of acid and base are maintained equal whereas the saline solution outlet flowrate is twice as high reaching up to 4.4 L $min^{-1}$. For values of chemicals outlet flowrates higher than 2.2, the saline solution outlet flowrate is maintained constant at 4.4 L $min^{-1}$. In the simulated conditions, the limiting current density, calculated as described in Section 3.1.1.2, was lower than 20 A $m^{-2}$, thus far from the actual applied current density. The results of the sensitivity analysis are reported in Fig. 9 in terms of key performance indicators.

The Current Efficiency (CE) shows a decreasing trend as the target concentration rises at fixed current density. Instead, it increases when the current density rises at constant target concentration. The decrease as the concentration rises could be easily explained: by increasing the sodium hydroxide target concentration at a constant current density the average concentration in the base channel increases. This in turn results in a greater concentration difference across the CEM (and similarly across the AEM) thereby intensifying the diffusive flux of hydroxide ions to the salt channel. The rise in current efficiency, at a constant target concentration, by increasing the current density is less intuitive. This phenomenon is strictly related to the simulated process configuration, in which both the outlet concentration and flowrate that pass through the stack remain fixed for the base stream. Therefore, when increasing the current density the EDBM system increases its productivity reducing the concentration of the base stream at the stack inlet. This has a positive effect on the current efficiency due to the lower average concentration of NaOH in the base channel, which decreases the diffusive phenomena across the CEM. At 600 A $m^{-2}$ the highest current utilization is observed, with values in the range 72–95 %, while, reducing the current density to 320 A $m^{-2}$, gives a CE between 38 % and 88 %.

The SEC depends directly on the voltage applied to the stack and

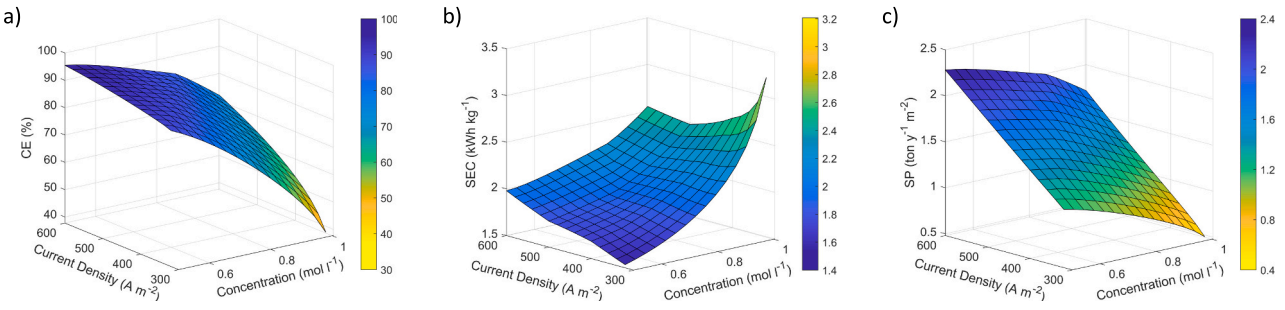


**Fig. 9.** Trends of key performance indicators, CE, SEC and SP, as function of current density and target concentration of sodium hydroxide.

inversely on the current efficiency. The voltage in turn shows an increase with the current density while its dependence on the base concentration is inversely proportional and quite weak. This is a consequence of the dominant resistance of the system which is the resistance of the cell packs. Overall, the SEC shows an increase with the concentration due to the dominant effect of the decreasing CE while its trend as a function of the current density is more complex because both voltage and CE play a counteracting role.

Two different trends of SEC as function of the current density are observed depending on the target concentration of sodium hydroxide. At low concentration (i.e, lower than 0.8 mol $L^{-1}$) an increasing trend with the current is observed, while a trend with a minimum is observed at a high concentration (i.e, higher than 0.8 mol $L^{-1}$). For low target concentration of sodium hydroxide the effect of the voltage is dominant in the SEC. In contrast both the effects of voltage and CE become significant at high concentrations and a minimum value is observed around 500 A $m^{-2}$. The minimum values observed for the SEC are in the range 1.5–2.5 kWh $kg^{-1}$ for target concentration between 0.5 mol $L^{-1}$ and 1 mol $L^{-1}$, respectively.

The SP behaviour is quite similar to that observed for the CE, as suggested by Eq. (3). Under a constant current density the SP and CE show a proportional relationship. When the current density is not fixed, the SP depends both on the CE and the current density. Maximum values between 2.3 ton $y^{-1}$ $m^{-2}$ and 1.7 ton $y^{-1}$ $m^{-2}$ are observed at 600 A $m^{-2}$, for sodium hydroxide concentration in the range 0.5–1 mol $L^{-1}$.

The economic analysis (Fig. 10) evaluates the LcoNaOH using the same operating conditions applied in the sensitivity analysis, considering variable current density and target concentration of NaOH. Additionally, the effect of varying the specific cost of electricity and the triplet cost on the LcoNaOH is examined for three different NaOH target concentrations, namely: 0.5, 0.75 and 1 mol $L^{-1}$.

The LcoNaOH rises with increasing concentration due to the decreasing CE of the process. At 320 A $m^{-2}$, the obtained values of LcoNaOH are in the range 310–680 € $ton^{-1}$, while lower values, in the range 290–370 € $ton^{-1}$, are observed at 600 $Am^{-2}$, for the entire range of concentration studied (0.5–1 mol $L^{-1}$). Raising the current density, a minimum can be identified for target concentrations lower than 0.86 mol $L^{-1}$, while a decreasing trend is observed for higher NaOH concentrations. The minimum lies between 500 A $m^{-2}$ and 560 A $m^{-2}$, with LcoNaOH values in the range 280–320 € $ton^{-1}$ (NaOH concentration in the range 0.5–0.86 mol $L^{-1}$). The observed minimum results from the counteracting effects of TEC and PC on the LcoNaOH. The TEC is associated with the SEC while the PC is linearly proportional to the SP. In fact, in the region of the low concentration values (< 0.8 mol $L^{-1}$), the SEC shows an increasing trend with the current density, which, in turn, produces an increase in the TEC. In the same region, the SP shows a growing trend with the current density, which produces an increase in the PC.

For high NaOH concentrations (> 0.8 mol $L^{-1}$), the TEC variation becomes dominant on the LcoNaOH especially at low current densities. On the other side, the PC shows an increasing trend with current density, resulting in a noticeable downward trend of LcoNaOH.

From Fig. 10b, c, d, it is evident that $E_p$ has a dominant effect on the LcoNaOH, while the triplet cost has a lower influence. Interestingly, in

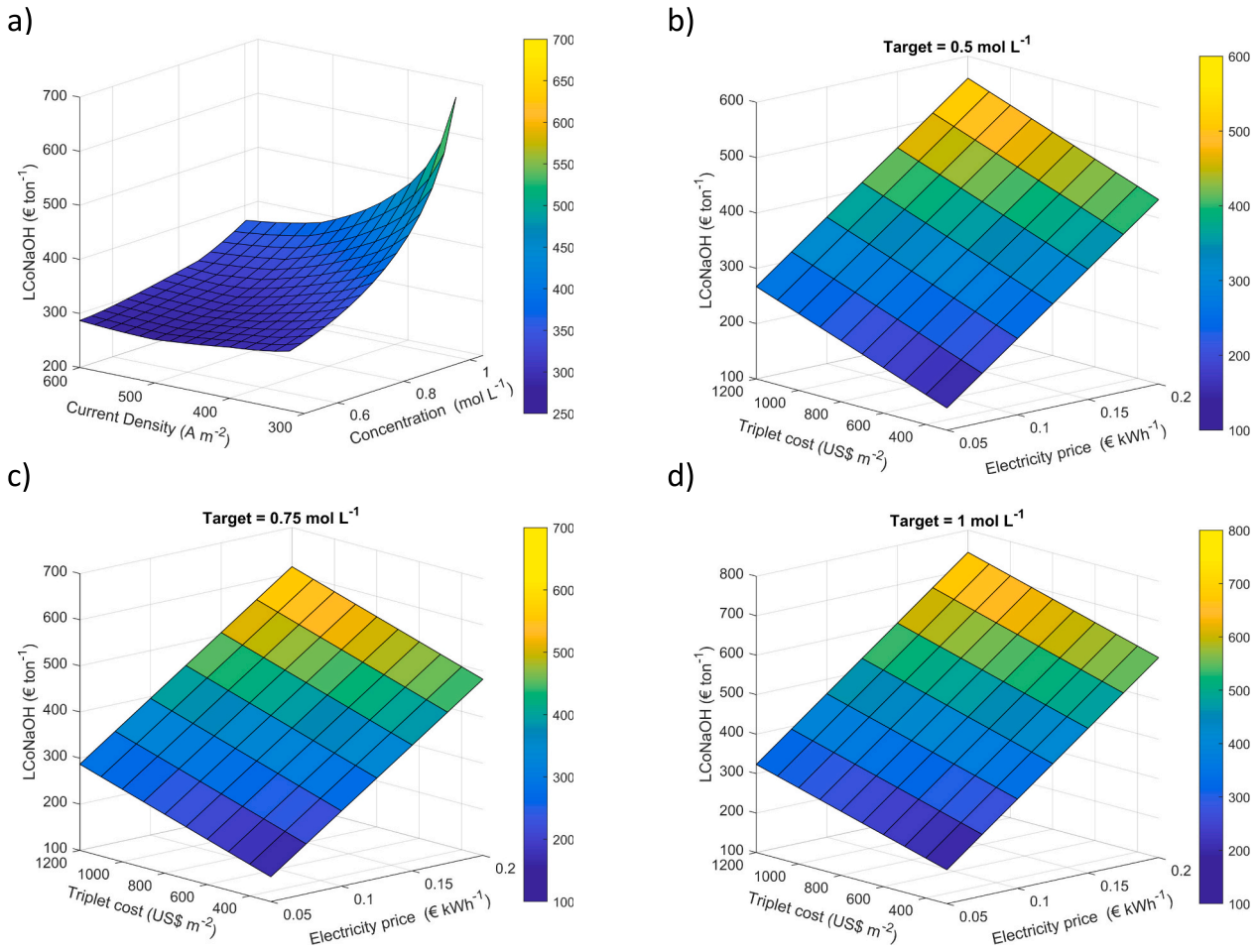


**Fig. 10.** a) Levelized cost of sodium hydroxide (LcoNaOH) as a function of NaOH target concentration and current density for a fixed triplet cost (600 US$ $m^{-2}$) and electricity price (0.1 € $kWh^{-1}$). b) Variation of LcoNaOH with electricity price and triplet cost, for the target concentration of 0.5 mol $L^{-1}$, c) 0.75 mol $L^{-1}$ and d) 1 mol $L^{-1}$. Current density is fixed to 500, 520 and 600 A $m^{-2}$, for cases b, c and d, respectively.

the most favourable conditions, indicating a scenario with low electricity and membrane costs, a production cost below 150 € $ton^{-1}$ of NaOH can be achieved when a target of 0.5 mol $L^{-1}$ is fixed, while increasing the target to 1 mol $L^{-1}$ the minimum in LCoNaOH rises to 180 € $ton^{-1}$. All that shows that the current price of membranes enables the production of valuable chemicals at a cost lower than the current market price of NaOH, ranging between 360 € $ton^{-1}$ and 680 € $ton^{-1}$ [47,48]. Moreover, the obtained production costs result comparable or even lower to those already reported in literature, in the range 340–370 € $ton^{-1}$ [28,49], for similar concentrations of sodium hydroxide.

#### 4.2.1. *Preliminary analysis of multi-stage EDBM potential*

As an example of use of the presented model for process intensification analysis, a double stage EDBM unit has been simulated in similar operating conditions. Specifically, two stacks with equal features as the one described in Section 2, are connected in serial arrangement as indicated in Fig. 11.

The same inlet concentrations and outlet flowrate ratio (described in Section 4.2) are employed for acid, base and salt line. The outlet streams from the first stack are directly sent to the second stack, while the flowrate in the recirculating loop is chosen to maintain the same channel speed in the two stacks (i.e., 2.6 cm $s^{-1}$).

The double stage configuration enables to distribute the concentration variation of the produced chemicals, in a way that the operating conditions of each stack can be optimize for that specific variation. In this case, the system is employed to produce 1 mol $L^{-1}$ NaOH, fixing the outlet concentration of each stack equal to 0.6 mol $L^{-1}$ and 1 mol $L^{-1}$ for the first stack and second stack, respectively. The choice of a higher concentration variation (from ~0 to 0.6 mol $L^{-1}$) in the stack 1, is due to the higher CE at lower concentration, which allows to produce more product in the first stage. The operating condition of the fist stack are those identified as optimal in the economic analysis above. For the second stack, inlet/outlet concentrations are fixed, while the current density is determined by the model itself.

The results of the analysis are reported in Table 7, showing a comparison with a single stage EDBM unit used to produce the same target. As expected, the first stage works much more efficiently than the single unit, due to the lower average concentration in the channels. Instead, in the second stage, a slightly poorer performance is observed, due to the higher average concentration inside the base channel (0.88 mol $L^{-1}$ compared to 0.83 mol $L^{-1}$). However, comparing the overall performance of the double stage with the single stage, an important improvement in all energetic performance indicators can be observed, with an 8 % reduction in SEC and a 4 % increase in CE. The SP shows a slight reduction (6 %), but this effect is attenuated by the doubled total membrane area. Finally, comparing the two configurations in terms of LCoNaOH, a reduction of 10 % is observed for the double stage, highlighting the benefits of using multi-stage EDBM to reduce the production cost of NaOH.

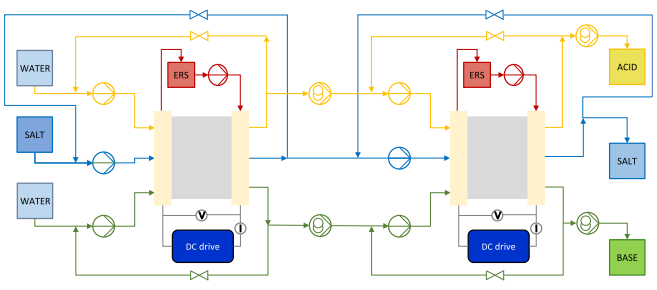


**Fig. 11.** Schematic representation of the simulated double stage EDBM's configuration.

## 5. Conclusions and future outlook

This work presents a comprehensive multi-scale model capable of simulating EDBM units for the in situ production of acid and base solutions. A complex stack configuration (i.e. internal staging), adopted for industrial application was simulated for the first time. The model was validated, adopting two process configurations (i.e., closed-loop and feed and bleed), with experimental data coming from a medium scale EDBM unit (i.e., total membrane area of 19.2 $m^2$), showing discrepancies of between 2 and 11 %. This validation allows the model to provide reliable results when simulating industrial scale stacks (e.g., a high number of triplets and elevated active membrane areas).

The internal staging configuration was analysed from an electrical point of view, deriving an ad hoc equivalent electrical circuit (i.e., stack model) to show current and voltage profiles along the entire stack. The effect of parasitic currents on the stack performance was analysed to understand if the linking manifold could promote this detrimental effect. It was observed that the unused current due to parasitic effects is 3.1 %, with maximum values in the range 4.5–4.7 % in the middle of each cell-packs. This proved the cost-effectiveness of this stack configuration in reducing this undesired effect and suggesting that higher number of triplet can be installed in each cell pack, maintaining reasonable parasitic losses.

A techno- economic analysis was conducted for the feed and bleed process configuration. The results suggest that the CE increases with the current density, at fixed target concentrations of sodium hydroxide. Values as high as 95.5 % were obtained at 600 A $m^{-2}$ with a target concentration of sodium hydroxide of 0.5 mol $L^{-1}$. Interesting, the specific energy consumption shows a minimum in the trend with the current density at elevated concentrations of base, which lies around 500 A $m^{-2}$, where a value of 2.5 kWh $kg^{-1}$ was obtained at 1 mol $L^{-1}$ of base.

The economic analysis evaluated the Levelized Cost of sodium hydroxide (LCoNaOH) at different process conditions changing the current density and the target concentration of sodium hydroxide. A minimum was observed in LCoNaOH as function of the current density at low target concentrations, which lies between 500 A $m^{-2}$ and 560 A $m^{-2}$. Instead for higher concentrations a decreasing trend was observed, with lowest values lying at 600 A $m^{-2}$. Finally, a LCoNaOH between 280 and 380 € $ton^{-1}$ depending on the target concentration was found. The effect of varying the electricity price and the triplet cost was considered for three different target concentration (0.5, 0.75 and 1 mol $L^{-1}$), showing that the electricity price has a major effect on LCoNaOH. At 1 mol $L^{-1}$, reducing the electricity price up to 0.05 € $kWh^{-1}$ allows to obtain a value of 240 € $ton^{-1}$ for LCoNaOH at fixed triplet cost (i.e., 600 US$ $m^{-2}$). While, diminishing also the triplet cost to 300 US$ $m^{-2}$ leads to a value of 190 € $ton^{-1}$.

The scale-up potential of the model were shown simulating a double stage EDBM unit with two stacks in series. The overall performance was compared with a single stage EDBM unit working at the same target concentration. The results showed that higher performance for the double stage, with a reduction of 10 % in the LCoNaOH. Finally, a value of 334 € $ton^{-1}$ was obtained, which results significant lower to the current market price for NaOH (i.e., between 360 € $ton^{-1}$ and 680 € $ton^{-1}$ [47,48]).

These results suggest that EDBM technology results as a competitive option for the in situ production of chemicals reducing the transportation costs, handling and storage issues. It is worthy of note that the figures obtained for LCoNaOH includes all the expenditures that are used to produce sodium hydroxide and, at the same time, hydrochloric acid is produced without consuming additional energy. Consequently, this price allows to obtain two useful chemicals, increasing the attractiveness of this technology.

Future works will focus on the coupling of EDBM with renewable energy sources to reduce the electricity price and nullify the fossil dependence of this environmentally friendly technology. To this end, a

**Table 7**
Comparison between single and double stage EDBM configurations for a target concentration of 1 mol $L^{-1}$ NaOH. The performances of each stage as well as the overall are reported for the base stream.

| EDBM configuration | Stage | Target (mol $L^{-1}$) | i (A $m^{-2}$) | SEC (kWh $kg^{-1}$) | CE (%) | SP (tons $y^{-1}$ $m^{-2}$) | LCoNaOH (€ $ton^{-1}$) |
|---|---|---|---|---|---|---|---|
| Single stage | – | 1 | 600 | 2.5 | 72 | 1.7 | 372 |
| Double stage | 1 | 0.6 | 500 | 1.8 | 90 | 1.8 | – |
| | 2 | 1 | 573 | 2.9 | 61 | 1.4 | – |
| | Overall | 1 | – | 2.3 | 75 | 1.6 | 334 |

fully dynamic model will be developed to assess and optimize EDBM performance when a variable energy source is available. Moreover, an optimization of the number of stage and operating conditions will be investigated for the multi-stage EDBM configuration, to minimize the production cost of NaOH.

## Abbreviations

| | |
|---|---|
| AEL | Anion exchange layer |
| AEM | Anion exchange membrane |
| BPM | Bipolar membrane |
| CE | Current efficiency |
| CEL | Cation exchange layers |
| CEM | Cation exchange membrane |
| CFD | Computational fluid dynamics |
| CL | Closed-loop |
| DC | Direct current |
| DSA | Dimensionally stable anode |
| EDBM | Electrodialysis with bipolar membranes |
| ERS | Electrodes rinse solution |
| F&B | Feed and bleed |
| ICI | Initial capital investment |
| KPI | Key performance indicators |
| LCoNaOH | Levelized cost of sodium hydroxide |
| PC | Process capacity |
| RO | Reverse osmosis |
| SEC | Specific energy consumption |
| SP | Specific productivity |
| TEC | Total energy consumption |

### *Symbols*

| | |
|---|---|
| $AEM_{cost}$ (US$ $m^{-2}$) | Anion exchange membrane cost |
| $A_m$ ($m^2$) | Active membrane area |
| $BPM_{cost}$ (US$ $m^{-2}$) | Bipolar membrane cost |
| $CEM_{cost}$ (US$ $m^{-2}$) | Anion exchange membrane cost |
| $C_{conv}$ (€ $US\$^{-1}$) | US$/€ conversion |
| $EPF_{cost}$ (€) | Electrodes and plates and frames cost |
| $E_p$ (€ $kWh^{-1}$) | Electricity price |
| $IM_{cost}$ (€) | Cell packs installed in the stack cost |
| $I_{ext}$ (A) | External current |
| $Maint_{cost}$ (€) | Maintenance cost |
| $M_{lt}$ (y) | Membranes and spacers lifetime |
| $N_1$ (−) | Number of triplets in the first cell pack |
| $N_2$ (−) | Number of triplets in the second cell pack |
| $N_{holes}$ (−) | Number of holes in the spacers |
| $N_s$ (−) | Number of stacks in series |
| $N_{tr}$ (−) | Number of triplets |
| $PE_{cost}$ (€) | Peripheral equipment cost |
| $PE_{lt}$ (y) | Peripheral equipment and electrodes lifetime |
| $PM_p$ (g $mol^{-1}$) | External voltage |
| $P_{lt}$ (y) | Project lifetime |
| $R_u$ (Ω) | Apparent electrical resistance of the stack |
| $S_{cost}$ (US$ $m^{-2}$) | Spacer cost |
| $TS_{cost}$ (€) | Total cost of the stack |
| $T_{cost}$ (US$ $m^{-2}$) | Triplet cost |
| $U_{ext}$ (V) | External voltage |
| $t_i$ (−) | Ion transport number |
| $C$ (mol $L^{-1}$) | Molar concentration |
| $D$ ($m^2$ $s^{-1}$) | Diffusion coefficient |
| $E$ (V) | Triplet membrane potential |
| $F$ (C $mol^{-1}$) | Faraday constant |

(*continued on next column*)

(*continued*)

| | |
|---|---|
| $I$ (A) | Generic current |
| $J$ (mol $m^{-2}$ $s^{-1}$) | Molar flux |
| $Q$ ($l/min^{-1}$) | Volumetric flowrate |
| $R$ (Ω) | Generic electrical resistance |
| $S$ ($m^{-2}$) | Generic section |
| $V$ (V) | Generic voltage |
| $i$ (A $m^{-2}$) | Current density |
| $j$ (%) | Discount rate |
| $l$ (m) | Generic length |
| $z$ (−) | Ion charge |

### *Greek letters*

| | |
|---|---|
| $\eta_I$ (%) | Unused current due to parasitic currents effect |
| $\sigma$ (S $m^{-1}$) | Electrical conductivity |

### *Subscripts*

| | |
|---|---|
| 0 | Initial (time zero) |
| *av* | Average |
| *cal* | calibration |
| *diff* | Diffusive |
| *down* | Lower branch |
| *f* | Final |
| *i* | Generic ion specie |
| *k* | Generic triplet in the stack |
| *l* | Solution line (i.e., *a*, *b* or *s*) |
| *m* | Membrane (i.e., AEM, CEM or BPM) |
| $m_i$ | Manifold (i.e., $m_1$ or $m_2$) |
| *ohm* | Ohmic |
| *tot* | Total |
| *up* | Upper branch |

## CRediT authorship contribution statement

**Giovanni Virruso:** Software, Methodology, Investigation, Formal analysis, Data curation, Conceptualization, Visualization, Writing – original draft. **Calogero Cassaro:** Investigation, Methodology, Visualization. **Andrea Cipollina:** Conceptualization, Methodology, Supervision, Writing – review & editing. **Alessandro Tamburini:** Writing – review & editing, Validation, Supervision, Project administration, Methodology, Funding acquisition, Conceptualization. **I. David L. Bogle:** Writing – review & editing, Validation, Supervision, Methodology, Conceptualization. **Giorgio D.M. Micale:** Writing – review & editing, Validation, Supervision, Resources, Project administration, Funding acquisition.

## Declaration of competing interest

The authors declare the following financial interests/personal relationships which may be considered as potential competing interests: Giorgio Micale reports financial support was provided by University of Palermo. If there are other authors, they declare that they have no known competing financial interests or personal relationships that could have appeared to influence the work reported in this paper.

## Acknowledgements

This project has received funding from the European Union Horizon 2020 research and innovation program under Grant Agreement no. 869474 (WATER-MINING-next generation water-smart management systems: large scale demonstrations for a circular economy and society). www.watermining.eu.

The authors are grateful to Dr. Bauer and Engr. Danz from FuMA-Tech GmbH (Germany) for the useful advice given for the correct operation of the EDBM unit.

## Appendix A. Supplementary data

Supplementary data to this article can be found online at https://doi.org/10.1016/j.desal.2024.117724.

## References

[1] M.H.-H.W.P. Buchel Karl Heinz, Industrial Inorganic Chemistry, Second, WILEY-VCH Verlag CmbH, 2003.
[2] A. Kumar, F. Du, J.H. Lienhard, Caustic soda production, energy efficiency, and electrolyzers, ACS Energy Lett. 6 (10) (2021) 3563–3566, https://doi.org/10.1021/acsenergylett.1c01827.
[3] Chlor-alkali industry review 2021-2022, Available: https://chlorineindustryreview.com. (Accessed 26 August 2023) (Online).
[4] P. ; F. T. ; C. L. C. ; L. ke, B. ; S. R. ; N. T. ; Z. E. ; B. R. Chlorine. Schmittinger, Ullmann's Encyclopedia of Industrial Chemistry. Wiley, 2003. doi: https://doi.org/10.1002/14356007.
[5] G.P. Thiel, A. Kumar, A. Gómez-González, J.H. Lienhard, Utilization of desalination brine for sodium hydroxide production: technologies, engineering principles, recovery limits, and future directions, ACS Sustain. Chem. Eng. 5 (12) (2017) 11147–11162, https://doi.org/10.1021/acssuschemeng.7b02276.
[6] S.S. Madaeni, S. Samieirad, Chemical cleaning of reverse osmosis membrane fouled by wastewater, Desalination 257 (1–3) (2010) 80–86, https://doi.org/10.1016/j.desal.2010.03.002.
[7] J.R. Davis, Y. Chen, J.C. Baygents, J. Farrell, Production of acids and bases for ion exchange regeneration from dilute salt solutions using bipolar membrane electrodialysis, ACS Sustain. Chem. Eng. 3 (9) (2015) 2337–2342, https://doi.org/10.1021/acssuschemeng.5b00654.
[8] F. Vassallo, et al., A pilot-plant for the selective recovery of magnesium and calcium from waste brines, Desalination 517 (2021), https://doi.org/10.1016/j.desal.2021.115231.
[9] Eusalt, Caustic soda uses, Available: https://eusalt.com/about-salt/salt-uses/industry/. (Accessed 26 August 2023) (Online).
[10] J. Shen, C. Zhao, G. Liu, C. Chen, Enhancing the performance on anaerobic digestion of vinegar residue by sodium hydroxide pretreatment, Waste Biomass Valoriz. 8 (4) (2017), https://doi.org/10.1007/s12649-016-9666-2.
[11] W. Ye, et al., Environmental evaluation of bipolar membrane electrodialysis for NaOH production from wastewater: conditioning NaOH as a CO2 absorbent, Sep. Purif. Technol. 144 (2015) 206–214, https://doi.org/10.1016/j.seppur.2015.02.031.
[12] M. Yoo, S.J. Han, J.H. Wee, Carbon dioxide capture capacity of sodium hydroxide aqueous solution, J. Environ. Manag. 114 (2013), https://doi.org/10.1016/j.jenvman.2012.10.061.
[13] H. Ruan *et al.*, "Capturing CO2 with NaOH solution from reject brine via an integrated technology based on bipolar membrane electrodialysis and hollow fiber membrane contactor," Chem. Eng. J., vol. 450, p. 138095, Dec. 2022, doi: https://doi.org/10.1016/j.cej.2022.138095.
[14] OxyChem, Hydrochloric acid handbook, Available: https://www.oxy.com/siteassets/documents/chemicals/products/chlor-alkali/Hydrochloric_Acid_Handbook.pdf. (Accessed 28 August 2023).
[15] Foodcom, Hydrochloric acid: applications in the food and pharmaceutical industries, Available: https://foodcom.pl/en/hydrochloric-acid-applications-in-the-food-and-pharmaceutical-industries/. (Accessed 15 October 2023).
[16] A. Culcasi, R. Gueccia, S. Randazzo, A. Cipollina, G. Micale, Design of a novel membrane-integrated waste acid recovery process from pickling solution, J. Clean. Prod. 236 (2019), https://doi.org/10.1016/j.jclepro.2019.117623.
[17] A. Mirwan, M.D. Putra, J.-C. Liu, A. Altway Susianto, R. Handogo, Aluminum leaching from water treatment sludge using hydrochloric acid and kinetic study, Environ. Sci. Pollut. Res. 27 (20) (2020) 25553–25562, https://doi.org/10.1007/s11356-020-08922-x.
[18] Purolite, "C104Plus and C104EPlus Hydrogen Cycle Operation Hydrochloric or Sulfuric Acid Regeneration.".
[19] H. Strathmann, Ion-exchange Membrane Separation Processes, First edit, Elsevier B.V, 2004.
[20] S.A. Mareev, et al., A comprehensive mathematical model of water splitting in bipolar membranes: impact of the spatial distribution of fixed charges and catalyst at bipolar junction, J. Membr. Sci. 603 (2020), https://doi.org/10.1016/j.memsci.2020.118010.
[21] H. Strathmann, Electrodialysis, a mature technology with a multitude of new applications, Desalination 264 (3) (2010) 268–288, https://doi.org/10.1016/j.desal.2010.04.069.
[22] Y. Tanaka, Ion Exchange Membranes: Fundamentals and Applications, Elsevier B. V, Amsterdam, 2007.
[23] R. Pärnamäe, et al., Bipolar membranes: a review on principles, latest developments, and applications, J. Membr. Sci. 617 (2021), https://doi.org/10.1016/j.memsci.2020.118538.
[24] X. Tongwen, Electrodialysis processes with bipolar membranes (EDBM) in environmental protection - a review, Resour. Conserv. Recycl. 37 (1) (2002), https://doi.org/10.1016/S0921-3449(02)00032-0.
[25] C. Cassaro, G. Virruso, A. Culcasi, A. Cipollina, A. Tamburini, G. Micale, Electrodialysis with bipolar membranes for the sustainable production of chemicals from seawater brines at pilot plant scale, ACS Sustain. Chem. Eng. 11 (7) (2023) 2989–3000, https://doi.org/10.1021/acssuschemeng.2c06636.
[26] M. Herrero-Gonzalez, et al., Analysis of operational parameters in acid and base production using an electrodialysis with bipolar membranes pilot plant, Membranes (Basel) 13 (2) (2023), https://doi.org/10.3390/membranes13020200.
[27] G. Virruso, C. Cassaro, A. Tamburini, A. Cipollina, G.D.M. Micale, Performance Evaluation of an Electrodialysis with Bipolar Membranes Pilot Plant Operated in Feed & Bleed Mode, 2023, https://doi.org/10.3303/CET23105013.
[28] A. Culcasi, L. Gurreri, A. Cipollina, A. Tamburini, and G. Micale, "A comprehensive multi-scale model for bipolar membrane electrodialysis (BMED)," Chem. Eng. J., vol. 437, p. 135317, Jun. 2022, doi: https://doi.org/10.1016/J.CEJ.2022.135317.
[29] A. Ortega, et al., Modelling water dissociation, acid-base neutralization and ion transport in bipolar membranes for acid-base flow batteries, J. Membr. Sci. 641 (2022), https://doi.org/10.1016/j.memsci.2021.119899.
[30] T. León, J. López, R. Torres, J. Grau, L. Jofre, J.-L. Cortina, Describing ion transport and water splitting in an electrodialysis stack with bipolar membranes by a 2-D model: experimental validation, J. Membr. Sci. 660 (2022), https://doi.org/10.1016/j.memsci.2022.120835.
[31] M.P. Mier, R. Ibañez, I. Ortiz, Influence of ion concentration on the kinetics of electrodialysis with bipolar membranes, Sep. Purif. Technol. 59 (2) (2008) 197–205, https://doi.org/10.1016/j.seppur.2007.06.015.
[32] S. Koter and A. Warszawski, "A new model for characterization of bipolar membrane electrodialysis of brine," Desalination, vol. 198, no. 1–3, pp. 111–123, 2006, doi: https://doi.org/10.1016/j.desal.2006.09.016.
[33] J.L. Gineste, G. Pourcelly, Y. Lorrain, F. Persin, C. Gavach, Analysis of factors limiting the use of bipolar membranes: a simplified model to determine trends, J. Membr. Sci. 112 (2) (1996) 199–208, https://doi.org/10.1016/0376-7388(95)00284-7.
[34] Y. Wang, A. Wang, X. Zhang, T. Xu, Simulation of electrodialysis with bipolar membranes: estimation of process performance and energy consumption, Ind. Eng. Chem. Res. 50 (24) (2011) 13911–13921, https://doi.org/10.1021/ie200467s.
[35] A. Culcasi, et al., Ionic shortcut currents via manifolds in reverse electrodialysis stacks, Desalination 485 (2020), https://doi.org/10.1016/j.desal.2020.114450.
[36] M. Reig, S. Casas, C. Valderrama, O. Gibert, and J. L. Cortina, "Integration of monopolar and bipolar electrodialysis for valorization of seawater reverse osmosis desalination brines: production of strong acid and base," Desalination, vol. 398, pp. 87–97, Nov. 2016, doi: https://doi.org/10.1016/j.desal.2016.07.024.
[37] R. Ibáñez, A. Pérez-González, P. Gómez, A.M. Urtiaga, I. Ortiz, Acid and base recovery from softened reverse osmosis (RO) brines. Experimental assessment using model concentrates, Desalination 309 (2013) 165–170, https://doi.org/10.1016/j.desal.2012.10.006.
[38] Y. Yang, X. Gao, A. Fan, L. Fu, C. Gao, An innovative beneficial reuse of seawater concentrate using bipolar membrane electrodialysis, J. Membr. Sci. 449 (2014) 119–126, https://doi.org/10.1016/j.memsci.2013.07.066.
[39] A. Culcasi, L. Gurreri, A. Zaffora, A. Cosenza, A. Tamburini, G. Micale, On the modelling of an Acid/Base Flow Battery: an innovative electrical energy storage device based on pH and salinity gradients, Appl. Energy 277 (Nov. 2020) 115576, https://doi.org/10.1016/j.apenergy.2020.115576.
[40] R. B. McCleskey, D. K. Nordstrom, J. N. Ryan, and J. W. Ball, "A new method of calculating electrical conductivity with applications to natural waters," Geochim. Cosmochim. Acta, vol. 77, pp. 369–382, Jan. 2012, doi: https://doi.org/10.1016/J.GCA.2011.10.031.
[41] H. Strathmann, J.J. Krol, H.-J. Rapp, G. Eigenberger, Limiting current density and water dissociation in bipolar membranes, J. Membr. Sci. 125 (1) (1997) 123–142, https://doi.org/10.1016/S0376-7388(96)00185-8.
[42] C. Lei, et al., Comparative study on the production of gluconic acid by electrodialysis and bipolar membrane electrodialysis: effects of cell configurations, J. Membr. Sci. 608 (Aug. 2020) 118192, https://doi.org/10.1016/J.MEMSCI.2020.118192.
[43] XE currency converter, Available: https://www.xe.com/currencyconverter/convert/?Amount=1&From=EUR&To=USD. (Accessed 16 August 2023) (Online).
[44] Eurostat, Electricity price statistics, Available: https://ec.europa.eu/eurostat/databrowser/view/NRG_PC_205/default/table?lang=en. (Accessed 15 August 2023) (Online).
[45] H.-J. Lee, F. Sarfert, H. Strathmann, S.-H. Moon, Designing of an electrodialysis desalination plant, Desalination 142 (3) (2002) 267–286, https://doi.org/10.1016/S0011-9164(02)00208-4.
[46] J.A.M.K. Kontturi, L. Murtomäki, Ionic Transport Processes, Oxford University Press, 2008. Available: https://oxford.universitypressscholarship.com/view/10.1093/acprof:oso/9780199533817.001.0001/acprof-9780199533817 (Online).

[47] W. Zhang, et al., Process economic evaluation of resource valorization of seawater concentrate by membrane technology, ACS Sustain. Chem. Eng. 5 (7) (2017) 5820–5830, https://doi.org/10.1021/acssuschemeng.7b00555.
[48] Y. Cao, M. Kasaeian, H. Abbasspoor, M. Shamoushaki, M.A. Ehyaei, S. Abanades, Energy, exergy, and economic analyses of a novel biomass-based multigeneration system integrated with multi-effect distillation, electrodialysis, and LNG tank, Desalination 526 (2022), https://doi.org/10.1016/j.desal.2022.115550.
[49] O.S.L. Bruinsma, D.J. Branken, T.N. Lemmer, L. van der Westhuizen, S. Rossouw, Sodium sulfate splitting as zero brine process in a base metal refinery: screening and optimization in batch mode, Desalination 511 (Sep. 2021), https://doi.org/10.1016/j.desal.2021.115096.